Design of an In-Situ Fuel, Oxygen, and Potable Water Supply System on Manned Mars Missions

A Capstone Report
presented to the faculty of the
School of Engineering and Applied Science
University of Virginia

by

Rahim Zaman

with

Craig Doody
Michael Mace
Spencer Plutchak
Sabrina Stenberg

May 5, 2020

On my honor as a University student, I have neither given nor received unauthorized aid on this assignment as defined by the Honor Guidelines for Thesis-Related Assignments.

Signed: _____

Approved: _____ Date _____
Eric Anderson, Department of Chemical Engineering

TABLE OF CONTENTS

1. Executive Summary

In-Situ Resource Utilization (ISRU) can negate the costs of shipping hydrogen, oxygen, and potable water to Mars. We propose a Martian ISRU system of unit operations to produce these resources and replace shipments from Earth. In our process, hydrogen is produced from the water-gas shift reaction, oxygen is produced from carbon dioxide reduction, and water is drilled from the regolith and desalinated. Oxygen and water production meet the life-support demands of ten colonists for one and a half year-long cycles, and the hydrogen and oxygen fuel are sufficient for a return trip to Earth. The process is powered by Kilopower generators, which use both nuclear fission and solar power to generate electricity. Our plant is expected to run for 18 years or 12 cycles. The system was modelled using Aspen Plus simulations combined with detailed reactor, separator, and ancillary equipment designs. Since equipment and materials have to be transported from Earth, accurate cost estimates are integral. Based on our calculations, the total process cost ranges from $1.6 billion to $7.6 billion, based on operation either remotely from Earth or by astronauts on Mars, respectively. If the same amount of fuel and potable water were to be shipped to Mars, it would cost $9.8 billion, so this proposed ISRU process is cost effective. The largest costs arise from the Kilopower units and CO_2 reducer catalyst because they have the highest mass requirements of the components in the process; future projects could work to optimize their masses. Overall, our proposed system is intended to contribute to ISRU research for manned missions and potential colonies on Mars.

2. Background and Motivation

The National Aeronautics and Space Administration (NASA), space agencies of other nations, and private companies plan to send humans to Mars in the next several decades. Such ventures will have great mission costs to achieve, with most of the cost as material and equipment transportation from Earth to Mars. According to a NASA report by Kleinhenz and Paz, shipping costs could be drastically cut with the use of In-Situ Resource Utilization (ISRU), which would utilize Martian resources for Mars base necessities (2017). These essentials include fuel for a return trip, as well as oxygen and water for a life support system. Based on a study by Shisko et al., the process must be economically viable to ensure adequate investment from stakeholders, which include space agencies, private enterprises, science communities, space enthusiasts, and colonists (2015).

ISRU optimizes the use of materials on the host planet, recycling where possible, as described by NASA (2019). Powell et al. explains how NASA has researched optimal ways to provide oxygen and water for a Martian colony, as well as sufficient hydrogen to fuel a rocket for their return trip (2001). Hydrogen can be obtained using the Water-Gas Shift (WGS) reaction and stored for later use, while the Mars Oxygen ISRU Experiment (MOXIE) is the current method proposed to produce oxygen, as reported by Meyen et al. (2016). As described by Hall, NASA has a current research project for the near-term technology called Kilopower, which is a 10 kWe fission powered reactor for space travel that would enable a long-term stay on Mars and support ISRU (2017). The International Space Station (ISS) is equipped with a closed-loop water recycling system that can filter impurities and contaminants out of wastewater in order to produce potable water; such a system would be practical on Mars, as described by Wiedemann (2014). Elon Musk and

SpaceX intend to send a preliminary cargo mission to Mars in 2022, followed by a cargo and crew mission in 2024. These two missions could establish a self-sustaining Martian colony with the means to provide their own power, mining, and life support (2016).

According to Ralphs et al., it is currently estimated that the Martian soil composition is up to 13% water, so brine can be extracted from the Martian surface (2015). Landing sites that NASA has considered in the past include Eberswalde, Mawrth Vallis, Arabia Terra, the Martian "glaciers" at Hellas Basin in Mars' mid-latitudes, and Valles Marineris (2019). Water extraction from Martian regolith is possible in various geographies on Mars, including the icy soils and permafrost at higher and lower latitudes and hydrated minerals from the equator; Ralphs et al. also propose a system to increase water extraction as a Martian colony expands (2015). Wasilewski offers an evaluation of drilling-based water extraction methods for Martian ISRU from mid-latitude ice resources, concluding that Honeybee's Auto-Gopher is the most efficient option for regolith and ice sampling due to its high efficiency rating, mature technological state, and lightweight design (2018).

Despite the drive to send humans to Mars, there are also debates against the human colonization of Mars or other astronomical bodies. As discussed by Smith et al., on an existential level, people debate that besides the moral duty of self-preservation, there could also be a "duty to allow our own extinction." In the same work, participants discussed how to distinguish between "a right to preserve humanity and a duty to preserve humanity" (2019). According to Munevar, humans have an obligation to colonize outer space for short-term goals, such as increasing the scientific knowledge base and accessing the resources that the solar system provides, as well as future goals such as "saving humanity from collisions with asteroids and other cosmic catastrophes"

(2019). In an article by Smith et al., a scholarly audience identifies the following ethical dilemmas for the colonization of space (2019):

> *"1 Is there a moral duty to preserve humanity through colonization?*
> *2 Is any such duty contingent on the good behavior of humanity?*
> *3 Is colonization, in the long run, a good or bad thing for Earth's other inhabitants?*
> *4 Given this discussion, what goals should we be pursuing w.r.t. colonization right now?*
> *5 What alternatives to the traditional model of colonization should we pursue?*
> *6 Is it morally permissible to send humans into what is likely to be a hellish situation?"*

To those of us content with our lives on Earth, it may seem like a waste of human and material resources to send mankind to Mars. However, it is tempting to be swayed by the influential scientists and astronauts who tell us that it is more or less a necessity to establish a Martian colony, including Buzz Aldrin, Stephen Hawking, Elon Musk, Bill Nye, and Neil deGrasse Tyson. According to Orwig, some compelling ethical and practical reasons to go to Mars are to ensure the perpetuity of humanity, possibly discovering simple biological life, improving life on Earth through serendipitous scientific innovation, galvanizing future generations to look towards space, and demonstrating the political and economical leadership of the United States by colonizing Mars first (2015).

This capstone design project consists of a continuous process that utilizes available Martian resources for production of output in an energy efficient way. Hydrogen is produced through the WGS reaction, which also produces carbon dioxide that can be recycled to increase hydrogen production. MOXIE generates the necessary oxygen for the colony. Water is mined from the ground as ice, melted, and desalinated through evaporation. NASA's Kilopower technology is used to power the process and the equipment that extracts materials from the atmosphere and regolith. A process flow diagram can be seen in Figure 2.1 and an overall material balance can be seen in Table 2.1.

The process is required to produce 2,222 kg of liquid hydrogen for fuel and 17,778 kg of liquid oxygen for fuel oxidizer for 20,000 kg of total propellant mass (Campbell, 2019). This is based on calculations for a 547 day mission with a 24 hr/day production period. As it is recommended for the return vehicle to be fuel rich, excess oxygen is produced, some of which is sent to the human habitat (Braeunig, 2012). The habitat is assumed to house ten astronauts for the current project (Campbell, 2019); the particulars of the habitat are outside the scope of this project. Excess water from the process is sent to the human habitat, but this amount is variable and dependent on habitat recycle flows, which are outside the scope of this project. In addition, a potential oxygen recycle system on Mars could use biological oxygen production, but this is also outside the scope of the current work (Hall, 2017).

The timescale for production is twelve 1.5-year cycles, or a total of 18 years, with 12,000 hours of operation (von Braun, 1965). Based on this timescale, the minimum product flow rates required are 0.2 kg/hr H_2 and 1.5 kg/hr O_2. Any amount above this is preferred to supply excess hydrogen fuel for the return vehicle and excess oxygen to the human habitat. In addition, having excess hydrogen and oxygen will protect our stored products from falling below required amounts due to total evaporation losses of 8.22 wt% over the 12,000 hour process lifetime (NASA, 2008). As such, our adjusted product flow rates are 0.3 kg/hr H_2, 2.4 kg/hr O_2, and 0.9 kg H_2O as seen in Table 2.1. These values are based on an Aspen simulation of the overall process that exceeds our production requirements to account for evaporation losses.

Based on our timescale, the minimum required water input for the process itself, excluding human water demand, is 1.9 kg/hr; our process uses 3.6 kg/hr. While we have found a source describing the amount of water needed to supply the habitat for daily use (5 kg/hr), such a flow rate

would increase our production rates far beyond what is needed (LaRC, n.d.). Our goal was to keep the equipment in Figure 2.1 as small as possible to reduce mass costs. Therefore, we chose to minimize water and oxygen as much as we could to reduce habitat recycle sizing.

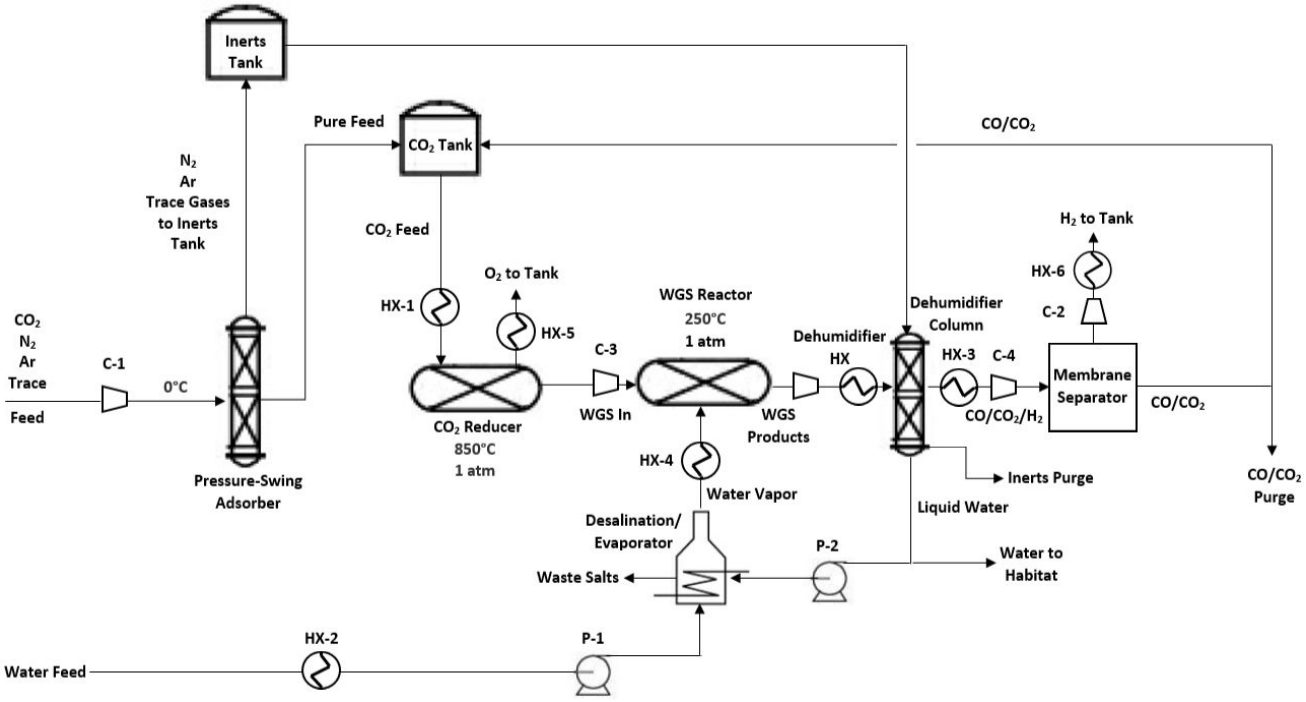

Figure 2.1. Process flow diagram of the Mars ISRU process

Table 2.1. Overall Process Stream Table

Component (kg/hr)	CO_2 Feed	H_2O Feed	O_2 Product	H_2 Product	Water Product	CO/CO_2 Purge
H_2	-	-	-	0.300	-	-
CO	0.001	-	-	-	-	0.006
O_2	-	-	2.385	-	-	-
CO_2	0.340	-	-	-	-	0.331
H_2O	-	3.623	-	-	0.942	-

Note: Table excludes inerts and salts separated from the inlet streams since they will all be separated before the reaction steps occur.

3. Process Design Discussion

3.1 Atmospheric Pressure-Swing Adsorber

Unit Overview

The CO_2 pressure swing adsorber removes inert components from the atmospheric feed to isolate CO_2 for the process. Table 3.1.1 describes the Martian atmosphere compression. The compression requires one compressor, elaborated later in the *Compressors and Pumps* section, to compress the gas in the two columns for adsorption. The gas fills one column with incoming atmospheric gas at 1 atm. The column's compressor then compresses the system to the 10 atm required for breakthrough (Walton & LeVan, 2006). The nitrogen (N_2) and argon (Ar) gases are allowed to pass into the inert storage tank. Next, the column is depressurized to 1 atm, emptied, cooled, and readied for the next rotation. The two-column design allows this process to remain continuous: one column fills and pressurizes while the other empties and cools (Wankat, 2012).

Table 3.1.1. Atmospheric Compression Stream Table

Component	Atmospheric Feed (kg/hr)	Inert Stream (kg/hr)	CO_2 Stream (kg/hr)
N_2	0.011	0.011	0.000
Ar	0.007	0.007	0.000
CO	0.001	0.000	0.001
CO_2	0.340	0.000	0.340

Shao et al. recommend a NaY sorbent (2009). However, to reduce weight, we chose to use an alumina-silica-sodia sorbent instead, as it reduces weight and increases absorptivity (Hussaro et al., 2008). Based on calculations of the required capacities, the columns themselves each contain

1.87 kg of sorbent and have dimensions of 0.18 m length and 0.06 m diameter. Although it is a packed bed, the column has negligible pressure drop across its length due to the small column length and the slow fluid velocity.

3.2 Carbon Dioxide Reducer

Design Layout

We chose to follow a NASA method that reduces carbon dioxide to produce oxygen on Mars (Walton & LeVan, 2006). The reduction reaction can be seen below.

$$2CO_2 \rightarrow 2CO + O_2$$

To run this reaction, we chose a tubular electrochemical reactor with a Yttria-Stabilized Zirconia (YSZ) catalyst. The reactor has three major regions. The first is the cathode, which consists of a YSZ network with additional nickel (Ni) binding sites. This cathodic region allows the CO_2 to bind to sites within the cathode and reduce to CO. The second region is the electrolyte made of denser YSZ, which, given an electric current, allows for ionization and transfer of atomic oxygen into the anode (Dipu et al., 2015). Since some of the oxygen is sent to the human habitat, presence of CO in that stream would be hazardous. However, the kinetics of the reaction govern that only the oxygen diffuses across the barrier, preventing CO contamination (Yurkiv et al., 2011). The final region of the reactor is the anode, which consists of YSZ catalyst with Lanthanum Strontium Manganite (LSM). Here, oxygen anions combine to form diatomic oxygen.

The reactor is set up such that the three regions are concentric layers in the reactor, with the outermost layer the cathode, the middle layer the electrolyte, and the inner layer the anode (Dipu et al., 2015). Figure 3.2.1 shows a rough schematic of the inside, along with an inducer jacket that provides heat to the system. The electricity is provided by platinum wires that travel along the length of the reactor (Dipu et al., 2015).

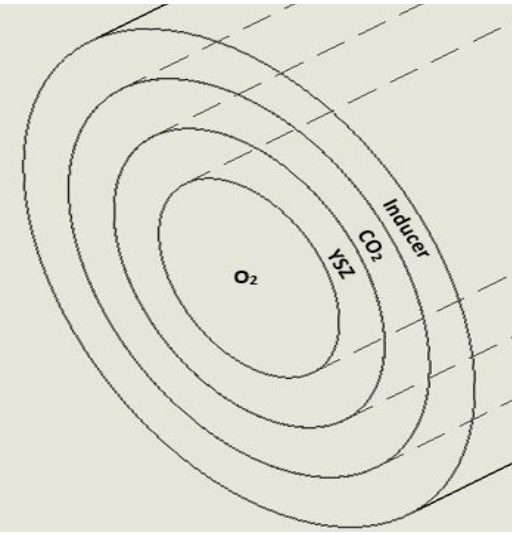

Figure 3.2.1. Cross sectional schematic of CO_2 reducer layers. Layers are not shown to scale.

Material Balance of the CO_2 Reducer

The material balance focuses on the production of oxygen in the system. The reducer needs to produce a minimum of 1.84 kg/hr O_2. It also needs to achieve a relatively high conversion of CO_2 to CO for the WGS reactor to run. After running a detailed Aspen material balance, we calculated the feed flow rates to be 6.63 kg/hr CO_2 and 0.12 kg/hr CO for this operation; this calculation included our real conversion, discussed later in this section, and the overall process recycle.

Although Aspen gave us 2 wt% CO in the feed, we chose to run reactor simulations with 5 wt% CO. There are two reasons for the inclusion of CO. The first is to account for the recycle stream. The CO/CO_2 recycle has CO present after the WGS exit stream, which enters the CO_2 tank over the lifetime of the factory; the 5 wt% CO accounts for this impurity. The second reason is to improve catalyst lifespan. Literature suggests that maintaining some CO in the reactor feed extends the lifetime of the catalyst. In fact, since there is no sulphur in our system - the main contaminant found in extended lifetime trials - and our catalyst maintains this reductive component, it is expected to last longer than the 500 h lifespan tested (Ebbesen & Mogensen, 2009).

To determine the reactor sizing and performance, we performed simulations using MATLAB® to obtain these values. We followed a Plug Flow Reactor (PFR) differential system of equations that relate conversion, temperature, and pressure to model the behavior and determine optimal operation conditions. These equations can be seen in Figure 3.2.2. The calculations were performed mainly on the cathode, as followed the precedent of other works (Dipu et al., 2015; Hu & Xie, 2019).

$$-u\frac{dC_i}{dz} = \eta_o \rho_B (-\upsilon_i)\mathrm{r} \qquad \text{(mass)}$$

$$u\rho \overline{C}_p \frac{dT}{dz} = (-\Delta H_r|_{T^0})\eta_o \rho_B (-\upsilon_i)\mathrm{r} - \frac{4U}{d_t}(T - T^*) \qquad \text{(energy)}$$

$$-\frac{dP}{dz} = \frac{f_f \rho u^2}{g_c d_p} \qquad \text{(momentum)}$$

$$C_i = C_i^0, \quad T = T^0, \quad P = P^0 \text{ at } z = 0$$

Figure 3.2.2. System of differential equations used to model the flow behavior of the reducer cathode (Davis & Davis, 2003).

Based on the simulations, the conversion is approximately 95%, so 2.38 kg/hr of O_2 is produced. This excess O_2 helps make up for the downtime of the process so O_2 is constantly provided to the habitat. Excess O_2 also mitigates losses due to evaporation that may occur during a cycle on Mars.

Dimensions of the CO_2 Reducer

Based on residence time calculations, the reducer has a length of 0.5 m and a diameter of 0.9 m. These allow the reducer to reach 95% conversion of CO_2 with a pressure drop of only 0.19 atm. The cathode is 0.5 m thick, the titanium shell is 0.01 m thick all around, and the electrolyte and anode layers each have a radial thickness of 0.2 m; these thicknesses are doubled to obtain the

diameter. The electrolyte layer only requires 5 mm of YSZ to provide the necessary protective diffusion. However, the thickness is 0.2 m to provide enough surface area for the desired conversion.

Energy Balance of the CO_2 Reducer

The reactor's PFR design creates a pressure drop across the column. Based on simulations of the fluid behavior, the reactor has a 0.14 atm pressure drop. Thus, the outlet streams exit at 0.86 atm. The electricity needs for the electrolyte were calculated by scaling the values provided by Dipu et al. Based on the current density and voltage described in their work for the chosen conditions, the power load of the reactor was calculated to be 1.23 kW (Dipu et al., 2015). The heating jacket provides the heat necessary to run the reaction and to maintain a temperature of 850 ^{o}C. Aspen simulations of the reactor calculated a duty of 11.7 kW to maintain these conditions. Having the inducer on the outside, however, would lead to massive radiative heat losses to the atmosphere. Thus, we decided to design an insulative layer using Multi-Layer Insulation (MLI) used by NASA. The MLI consists of 1 mm thick layers of aluminized Mylar, which helps reduce both conductive and radiative losses (Dunmore, n.d.). The insulation consists of 37 layers of MLI, which reduces the energy loss to only a few watts (Ross, 2015).

Kinetics of the CO_2 Reducer

Information on the kinetics of the reducer came from multiple sources. Research by Yurkiv et al. provided individual mechanisms for different interactions on the catalyst surface inside the reducer (2011). These included cathodic interactions and electron transfer in the electrolyte. However, the research did not provide an overall rate law, rates for binding with the Ni and YSZ sites in our cathode, or anode rate components (Yurkiv et al., 2011). Further information was

needed to determine the mechanism of the overall reduction process. The rate determining step was found to be the binding of CO_2 to the YSZ catalyst surface (Yin et al., 2019). We also found in the literature that Ni provides the important binding sites for the catalyst (Hu & Xie, 2019). The final component that was needed was the anode behavior, which was found in Meyen et al. with the necessary recombination (2016). The mechanism for the rate law was constructed with this information.

Figure 3.2.3 shows the overall mechanism as determined from the literature. The use of asterisks for binding sites follows the mechanism notation in Davis and Davis (2003). It begins with binding of CO_2 to available Ni binding sites ($*_{Ni}$). After the CO_2 binds to a nickel site (CO_2*_{Ni}), it combines with a second free binding site to allow the formation of bound carbon monoxide ($CO*_{Ni}$) and bound atomic oxygen ($O*_{Ni}$). The bound CO desorbs from the catalyst surface and frees up a binding site for another CO_2 molecule. The oxygen then transfers to the electrolyte and ionizes ($O^{-}*_{YSZ}$). The oxygen further ionizes as it travels through the electrolyte ($O^{2-}*_{YSZ}$). Finally, the oxygen anions combine to form molecular oxygen (O_2) and free up catalyst sites for further diffusion.

$$(1)\ CO_2 + *_{Ni} \rightarrow CO_2 *_{Ni}\ \ (RDS)$$
$$(2)\ CO_2 *_{Ni} + *_{Ni} \rightleftharpoons CO *_{Ni} + O *_{Ni}$$
$$(3)\ CO *_{Ni} \rightleftharpoons CO + *_{Ni}$$
$$(4)\ O *_{Ni} + e^- + *_{YSZ} \rightleftharpoons O^- *_{Ni} + *_{Ni}$$
$$(5)\ O^- *_{YSZ} + e^- \rightleftharpoons O^{2-} *_{YSZ}$$
$$(6)\ 2O^{2-} *_{YSZ} \rightleftharpoons O_2 + 4e^- + 2 *_{YSX}$$

Figure 3.2.3. Mechanism of CO_2 reduction derived from literature.

The rate constants and effective equilibrium constants for these steps were calculated from thermodynamic parameters provided by Yurkiv et al., which are found below in Table 3.2.1.

(2011). The derived equations for the mechanism were used to construct an overall rate expression, Equation 3.2.1.

Table 3.2.1. Molar Enthalpies and Entropies of Reactive Species in the CO_2 Reducer

Species	H_i (kJ/mol)	S_i (J/(mol*K))
CO	-84	238
CO_2	-353	275
Ni*	0	0
CO*Ni	-197	193
CO_2*Ni	-394	205
O*Ni	-222	39
YSZ*	0	0
O^-*YSZ	-236	0

Equation 3.2.1: $$r = r_{Rate\ Determining} = \frac{k_{f,2}[CO_2][Ni*]_0}{1 + (\frac{[O_2]}{K_3})^{1/2} \frac{[CO]}{K_1 K_4 K_{01}} + \frac{[CO]}{K_1} + (\frac{[O_2]}{K_3})^{1/2} \frac{1}{K_{01}}}$$

Heat Transfer within the CO_2 Reducer

The heat transfer rate of the CO_2 and CO mixture stream was determined through the Nusselt number (Equation 3.2.3), which is a function of the Reynolds (Equation 3.2.2) and Prandlt numbers. The velocity of the stream was calculated to be 2.14 x 10^{-2} m/s based on the research of Dipu et al. (2015). This value remained the same in the design of our CO_2 reducer. The Reynolds number was then determined from the tube diameter of 0.5 m and a kinematic viscosity of 9.324 x 10^{-5} m^2/s, which was determined through simulation of the mixture in Aspen. Aspen also provided the Prandtl number for our Nusselt number approximation, as well as the thermal conductivity (k) value for the convective heat transfer coefficient.

Equation 3.2.2: $Re = \frac{vd}{\nu}$

Equation 3.2.3: $Nu = 0.023 Re^{0.8} Pr^{0.3}$

Equation 3.2.4: $h = \frac{k}{d}(Nu)$

Materials of Construction and Insulation of the CO_2 Reducer

The reducer is made of titanium because it provides the necessary strength for the weight of the catalyst, and is able to hold up to the heats of the reaction and heating jacket (Green and Perry, 2018). An Electroheat IJ-Q heating jacket is used, which consists of a 100 mm thick quartz glass insulation jacket inside a proprietary carrier assembly (ElectroHeat, 2020). The jacket will extend past the reactor and onto the feed to preheat the reactants. Our preheating exchanger will only get the reactants to 690 ºC, so the jacket will help it reach reactor temperature at the beginning.

3.3 Water Evaporation/Desalination Unit

A combined evaporator and desalination unit is used to purify the water drilled from the Martian regolith for use in the WGS reaction. The water is extracted as ice and then preheated from -60 ^{o}C to 20 ^{o}C in a heat exchanger (*Heat Exchangers* Section). It then enters the evaporator and desalination unit at 4.39 kg/hr with the recycled liquid water stream, which is at 70 ^{o}C and enters at 4.59 kg/hr. The assumed composition of the extracted and liquefied water is shown in Table 3.3.1 and was modelled using the Elec-NRTL model in Aspen (Clark and Van Hart, 1981).

Table 3.3.1. Assumed Composition of Liquefied Martian Water Mixture

(Clark and Van Hart, 1981)

Component	Weight Percent
H_2O	82.50
$MgSO_4$	5.75
Na_2SO_4	5.75
$MgCO_3$	2.50
$CaCO_3$	2.50
NaCl	1.00

The unit is constructed from NASA-427 aluminum alloy to minimize corrosion from the 17.5 wt% salt water extracted from Mars (NASA, 2016). This aluminum alloy contains minor amounts of copper, manganese, iron, zinc, magnesium, and titanium balanced with aluminum (Lee, 2016).

The evaporator and desalination unit is modeled as a flash process. Based on equations from Wankat (2012), the dimensions of the unit are 0.3 m diameter and 0.6 m height, resulting in a heat

transfer area of 0.58 m^2. The element operates at 115 ºC and 1 atm to optimize the amount of water recovered, which requires 5.2 kW of power for heating based on Aspen simulations. By operating the unit at 115 ºC, all the water is evaporated and sent to the WGS reactor as water vapor. The heating is provided through a 45 L capacity, electrically-powered BriskHeat copper heating jacket (BriskHeat, 2020). The use of a heating jacket ensures easy regular cleaning of the tank. The electricity requirement for the heating is met through the use of Kilopower reactors.

The salts are fully separated from the water into a waste salt stream, so the water vapor product stream is of 100% purity, as determined through Aspen simulations. The salt mixture output from the unit is discarded at 0.77 kg/hr onto the Martian surface, as it has little use elsewhere in the process and cannot be allowed to accumulate in the system over time. The water vapor product stream is sent to the WGS reactor at 8.21 kg/hr.

3.4 Water-Gas Shift Reactor

This reactor runs the water-gas shift (WGS) reaction, which is as follows:

$$CO + H_2O \rightleftharpoons CO_2 + H_2$$

The selected reactor design is a 0.2 m long, 0.2 m diameter plug flow (packed bed) reactor with a CuO based catalyst. The chosen catalyst is ICI Catalyst 52-1, which is composed of 32% CuO, 53% ZnO, and 15% Al_2O_3 and has the empirically derived rate expression $r = kp_{CO}^{\alpha}p_{H_2O}^{\beta}$ (Salmi & Hakkarainen, 1989). The catalyst has a density of 5.38 g/cm^3 and a pore radius of 8.5 nm. Cu/Zn/Al catalysts, when used for the WGS reaction, usually have lifespans that last several years and eventually deactivate due to overexposure to sulfur (King & McLennan, 2010). The expected sulfur content of the feedstreams to this reaction is near zero, so the initial catalyst should last the entire 12,000 operation hours.

Excess water is fed to the reactor to increase conversion; the reaction stoichiometry is 1:1. The conversion of CO is 98.4% and the conversion of water is 55.9%. The desired product for rocket fuel is hydrogen, which is separated from the other products two steps later through the membrane separator unit. The unit's length and diameter were determined by testing sensitivity in MATLAB® for maximum conversion at a working flow rate.

The calculations have made the following assumptions. Operation is at steady-state. There are no changes in fluid density or transport limitations at this rate, so the overall effectiveness factor (η_0) is unity. The ideal particle size for a fixed bed reactor is between 2 and 5 mm, so a catalyst particle diameter of 2.4 mm is selected (Peters et al., 2003). Typical void fractions of packed beds range from 30-80% depending on the packing orientation, so 50% was chosen for this model (Eigenberger, 2000). Assuming that the functional, non-void space volume of the reactor is filled

with the catalyst, the mass of catalyst required is 18.3 kg. Calculations and computations were undertaken using a combination of Aspen and MATLAB®.

Momentum Balance of the WGS Reactor

The pressure drop throughout the length of the reactor (0.0 to 0.2 m) is 0.13 atm (1 to 0.87 atm). This pressure drop is accounted for with a compressor.

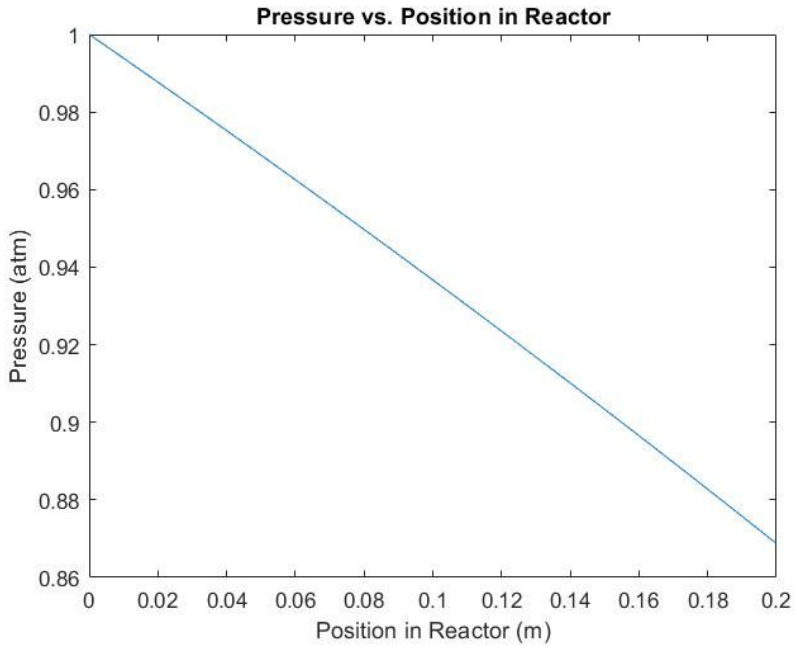

Figure 3.4.1. Pressure drop over the WGS reactor

Material Balance of the WGS Reactor

Operation of the WGS reactor is at 1 atm and the gaseous mixture of CO_2, CO, and water vapor is preheated to 250 ℃ prior to entering the reactor. The inlet and outlet flow rates can be seen below in Table 3.4.1. The reactor runs with excess water to increase the conversion of CO, which increases the production of H_2; the fractional conversion of CO and H_2O across the reactor can be

seen in Figure 3.4.2 below. It is necessary to produce excess hydrogen fuel in addition to oxygen because liquid oxygen/liquid hydrogen rockets perform best when fuel rich (Braeunig, 2012).

Table 3.4.1. Water-Gas Shift Reactor Stream Table

Component (kg/hr)	WGS Feed	H_2O Inlet	WGS Products
H_2	0.00	0.00	0.30
CO	4.30	0.00	0.13
CO_2	0.07	0.00	6.62
H_2O	0.00	8.21	5.53

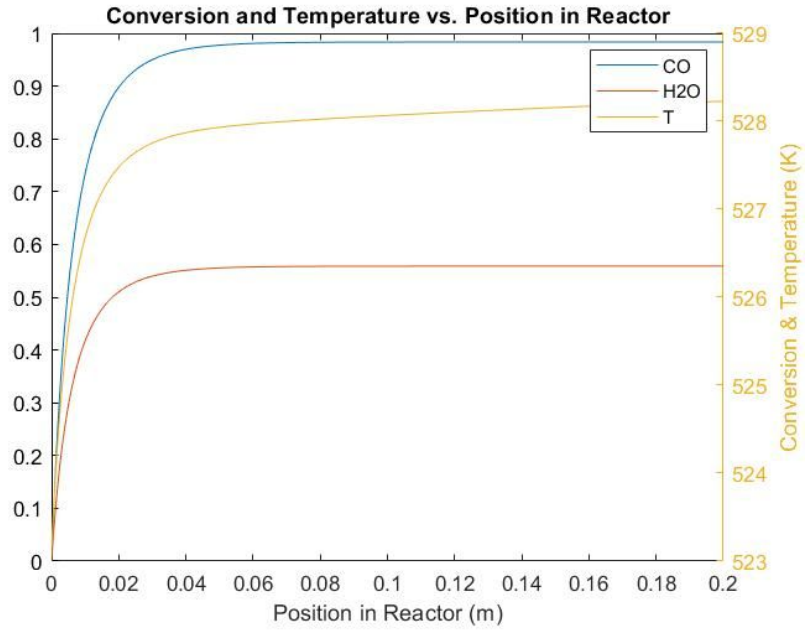

Figure 3.4.2. Fractional conversion and temperature of reaction mixture over the reactor length

Energy Balance of the WGS Reactor

The initial temperature of the inlet stream is 250 ℃. The temperature in the reactor reaches a maximum of 255 ℃ at 0.2 m, the end of the reactor. This temperature profile can be seen above in

Figure 3.4.2. The temperature is later lowered by 5 ℃ before it enters the dehumidifier and the pressure remains constant.

The overall heat transfer coefficient, U, of the reaction vessel was calculated by combining the heat transfer properties of the reaction stream, the titanium reactor walls, and a high temperature heat transfer fluid. Material properties of Dynalene 600 industrial heat transfer fluid were assumed for calculations. At 250 °C, titanium has a thermal conductivity of 20 W/mK, and the heat transfer fluid is assumed to have a heat transfer coefficient of 14.25 W/m^{2}K. Based on the assumption that the walls are 4 mm thick, the changing value of U can be represented as shown in *Equation 3.4*, where $h_{reaction}$ is the heat transfer coefficient of the reaction stream calculated from the stream variables.

Equation 3.4: $U = (h_{reaction}^{-1} + \frac{0.004}{20} + 14.25^{-1})^{-1} \frac{W}{m^2K}$

A cooling fluid temperature of 200°C is used to sufficiently counteract the heat of reaction and contain the rise in temperature to 5°. The overall cooling duty requirement is 0.04 kW.

Kinetics of the WGS Reactor

The WGS reactor runs the following reaction:

$$CO + H_2O \rightleftharpoons CO_2 + H_2$$

Every component is produced or consumed in a 1:1 molar ratio in this stoichiometry. In order to increase conversion of this reaction, excess water is fed to the reactor. The desired product is hydrogen for rocket fuel. The heat of reaction is 41.1 kJ/mol (Loganathan et al., 2010).

The chosen catalyst is ICI Catalyst 52-1, which is composed of 32% CuO, 53% ZnO, and 15% Al_2O_3 and has the empirical derived rate expression $r = kp_{CO}^{\alpha} p_{H_2O}^{\beta}$ (Salmi & Hakkarainen, 1989). The coefficients are as follows: $k = 4.40\ x\ 10^{-5} mol/(m^2 * s * atm)$, $\alpha = 1.07 \pm 0.16$, and

$\beta = 0.55 \pm 0.18$ (Salmi & Hakkarainen, 1989). The density of ICI Catalyst 52-1 is 5.83 g/cm^3 (Smith et al., 2010) and its BET surface area is 90 m^2/g (Twigg, 2018). The chosen equilibrium constant is $K_{eq} = exp(4577.8/T - 4.33)$ (Callaghan, 2006).

Materials of Construction and Insulation of the WGS Reactor

The chosen material of the WGS reactor is titanium, which was selected because it is both light and durable. Despite being more expensive than other options such as aluminum or steel, its weight to strength ratio allows less material to be used, offsetting the expense with a decrease in shipping cost. The total mass of the reactor is 21 kg, which includes both the weight of the titanium walls (2.7 kg) and of the catalyst packing (18.3 kg).

3.5 Dehumidifier

Components

The dehumidifier system consists of three components. The first is a compressor to reach atmospheric pressure, the design of which can be found in the *Compressors and Pumps* section. The second component is a heat exchanger that cools the effluent of the WGS reactor. This cooling causes the outlet stream to approach its dew point, easing the removal of water. The third component is a desiccant column that removes water, such that it can be recycled to the WGS reactor or sent to the human biome. Removing as much water as possible from the stream prevents ice formation in locations where liquid nitrogen is used for cooling.

Heat Exchanger Design

The heat exchanger is designed as a double pipe heat exchanger. Based on the flow rates, it was determined that multiple pipes would be unnecessary for the required heating. The hot stream is the WGS outlet stream, which has a flow rate of 12.59 kg/hr. Based on Aspen simulations, the stream enters the exchanger at 280 ^{o}C and cools to 107 ^{o}C. The cold stream is liquid nitrogen with a flow rate of 18.79 kg/hr to achieve the desired cooling. Based on heuristic heat transfer calculations from Peters et al. (2003), we determined that a double pipe heat exchanger requires a heat transfer area of 0.03 m^2 when it is 0.10 m long.

The material of choice is a nickel alloy due to the weight constraints of the process and the temperature of the hot stream. We used liquid nitrogen to minimize cooling fluid masses, and to instigate condensation. We could have used our glycol/water solution, which is described in the *Heat Exchangers* section, but that would have required the same amount of liquid nitrogen for cooling the glycol/water solution later in the process. The liquid nitrogen could cause freezing in

the tubes beyond the condensation we desire, so better heat integration with a different cooling stream is recommended.

Desiccant Column Design

The desiccant columns remove the remaining water from the stream which enters the hydrogen membrane separator. First, a column is filled with the incoming vapor stream and the water adsorbs to the desiccant. Zeolite 3A was chosen for the desiccant because it provides the best adsorptivity under our expected conditions (Grace-Davidson, 2010). The remaining gas passes through the column to the membrane separator for further processing. Once the water is adsorbed, the column is allowed to depressurize, allowing the water to desorb, condense, and feed into the dehumidifier (Lalik et al., 2006). Finally, the column is heated to remove any remaining water on the zeolite, and then regenerated with inert gases to prepare for the next rotation. The inert gases are the nitrogen and argon stored from the initial atmospheric separation, and used to dry the zeolite. Two columns are required: one is filled and compressed while the other is emptied and regenerated.

The desiccant column is designed to contain 0.31 kg of sorbent, which is enough to support one hour of water supply. This results in column dimensions of 0.18 m in length and 0.06 m in diameter. Because of the small column size, 1 mm particles of the zeolite were chosen. A pressure drop across the column was calculated using methods from Wankat (2012), but found to be negligible. The chosen material of construction is aluminum because the temperatures are moderate enough for its use.

3.6 Membrane Separator

Separation of H_2 from the $CO/CO_2/H_2$ Dehumidifier Outlet Stream

A palladium based membrane is used to separate the H_2 from the mixed CO (0.13 kg/hr), CO_2 (6.63 kg/hr), and H_2 (0.30 kg/hr) dehumidifier outlet stream. Palladium membranes typically consist of a continuous coating of palladium powder on a porous metal support tube. In the membrane, H_2 gas adsorbs onto the membrane surface, dissociates into atomic hydrogen, diffuses through the membrane, recombines into H_2, then desorbs on the other side of the membrane (Sanchez et al., 2013). A schematic of a palladium membrane can be seen in Figure 3.6.1.

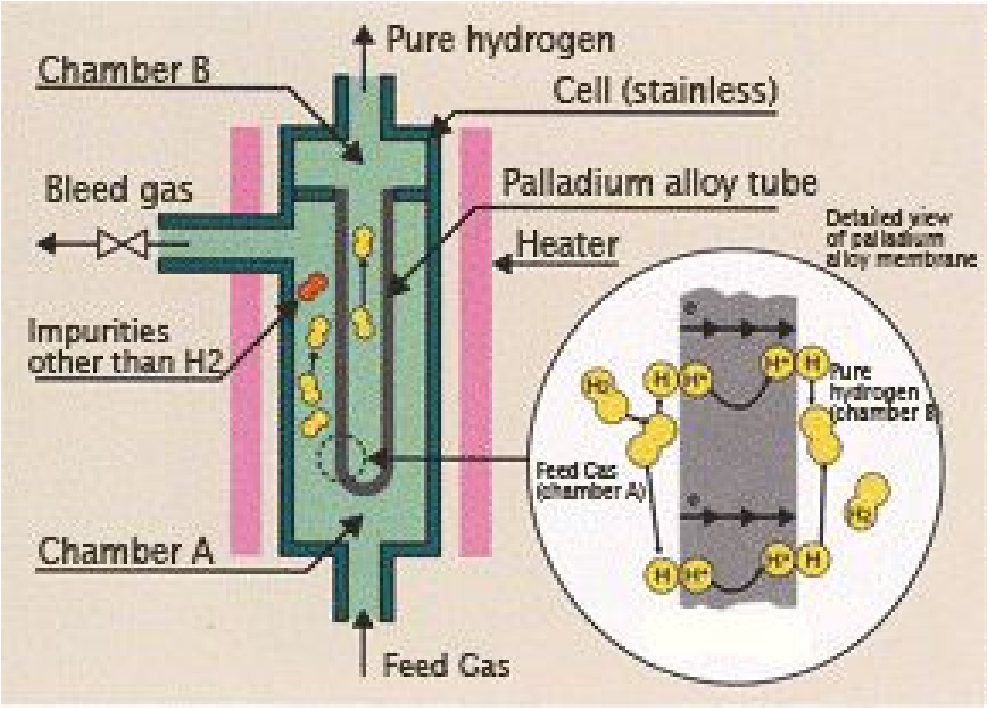

Figure 3.6.1. Palladium based H_2 separation membrane. The process of hydrogen transport through the membrane is shown in the detailed view (Japan Pionics Co.).

Design Specifications

Despite achieving pure hydrogen separation in a stream of CO_2, CO, and H_2, pure palladium membranes suffer from decreased permeation of hydrogen due to the competition for active sites between H_2 and CO_2 and the deposition of CO_2 onto the membrane surface. Additionally, dissociated hydrogen and carbon dioxide can react on the palladium surface to cause minor methanation and reverse water gas shift reactions to occur, leading to additional products that would require removal downstream. As a result, a 50/50 mol% mixture of CO_2 and H_2 passing through a pure palladium membrane yields only about 33 wt% of the feed hydrogen in the permeate (Sanchez et al., 2013). However, alloying of palladium with 7 wt% yttrium has been found to increase hydrogen permeability through the membrane by up to four times through increasing the interstitial spacing of the palladium (Burkhanov et al., 2011; Paglieri and Way, 2006). Such alloying also makes the aforementioned side reactions negligible (Mejdell et al., 2009). Due to these factors, a 93 wt% palladium, 7 wt% yttrium alloy powder on a porous stainless steel support tube is used to separate H_2 in the current process. This results in separation of H_2 by the membrane with a permeate stream of 0.3 kg/hr H_2 and a retentate stream of 6.63 kg/hr CO_2 and 0.13 kg/hr CO. A small amount of hydrogen will likely remain in the retentate stream due to incomplete permeation caused by mass transfer limitations. An increase in the feed pressure or inclusion of other separation elements would reduce the hydrogen content in the retentate stream. However, the current project assumes a retentate hydrogen content of zero based on the findings of Sanchez et al. (2013).

The presence of CO in the feed stream can severely degrade the membrane performance as strong CO adsorption on the membrane surface blocks active sites. However, it has been found that

this effect is negligible at feed temperatures greater than or equal to 450 °C (Sanchez et al., 2013). Thus, the membrane feed stream is heated from 288 °C to 450 °C using a 1.5 kW IJ-G electric heating jacket from ElectroHeat which consists of a 100 mm thick silk glass insulation jacket inside a proprietary carrier assembly prior to entering the membrane. In addition, a pressure drop of 0.5 atm is recommended for optimal H_2 permeate flux, so the membrane inlet in the current process is pressurized to 1.5 atm (*Compressors* Section) and drops to 1 atm in the permeate (Sanchez et al., 2013). Due to this pressure drop, permeability of 11.2 $m^3/(m^2*hr*kPa^{0.5})$, and permeate H_2 flux of 85.68 $m^2/(m^2*hr)$ are determined through the findings of Sanchez et al. and Burkhanov et al. The required thickness of the porous stainless steel support tube is calculated to be 0.3 m using Sievert's Law, Equation 3.6 (Sanchez et al.). In the Equation $n_{H_2,per}$ is the mass flux of the hydrogen permeate, P_{H_2} is the permeability of hydrogen in the membrane, $P_{H_2,ret}$ and $P_{H_2,per}$ are the pressures of the retentate and permeate, respectively, and *t* is the porous stainless steel support tube thickness or diameter.

$$\text{Equation 3.6: } n_{H_2,per} = P_{H_2} \frac{(P_{H_2,ret}{}^{0.5} - P_{H_2,per}{}^{0.5})}{t}$$

Based on the hydrogen permeate flux and permeate flow rate, the required surface area of the inner membrane tube is 0.1 m^2 and, subsequently, the required tube length is 0.1 m. Based on the work of Alique et al., the palladium-yttrium alloy powder layer on the support tube is 13 μm thick to achieve high hydrogen permeability and membrane stability (Alique et al., 2017). The membrane tube is housed in the piping leading to the CO/CO_2 purge valve.

3.7 Heat Exchangers

Heat Management

The process uses ten heat exchangers to reuse heat already in the process and minimize the need for electric heating, which saves electricity for other parts of the process. Table 3.7.1 below shows a summary of the non-compression heat exchangers in the process along with stream temperature changes, materials of construction, heat duty, and dimensions. The compression-related exchangers are in Table 3.7.2 with the same information. Apart from exchanger 1 in Table 3.7.1 and exchangers 7 and 8 in Table 3.7.2, which are shell and tube heat exchangers, all other heat exchangers are double pipe exchangers. In most cases, our fluid volumetric flow rates required little surface area and therefore only a single transfer surface. Calculations were performed with MATLAB® and heat transfer coefficient (U) heuristics: 850 W/m^2K for exchangers with phase changes and 30 W/m^2K for all other gas exchangers (Peters et al., 2003).

Heat exchangers 1 and 3 in Table 3.7.1 pre-heat their related unit operations. The reducer outlet on the cathode side leaves at 850 °C, then heats the reducer inlet stream to 690 °C; the reactor duty will minimally heat the inlet for proper reaction conditions. For heat exchanger 3, the hydrogen product stream of the membrane heats the incoming mixed stream. While the heat exchanger itself does not reach the needed 450 °C for the membrane separator, it does reduce the inlet heater duty.

Heat exchangers 2 and 4 in Table 3.7.1 use heat integration for the water components in the process. Exchanger 2 uses the 850 °C oxygen product stream from the CO_2 reducer anode to heat the incoming ice in our process. The hot stream has enough energy to heat and melt the ice, and

preheat the water entering the evaporator. Exchanger 4 cools the carbon stream that leaves the membrane separator and preheats the water vapor stream that exits the evaporator.

Heat exchangers 5 and 6 in Table 3.7.1 cool the desired products before storage. Both require cryogenic conditions, so cooling is provided by liquid nitrogen (LN_2). Exchanger 5 comes after exchanger 2 to minimize the flow rate of liquid nitrogen needed to cool and liquify the oxygen. By cooling the oxygen stream earlier in the process, exchanger 2 only requires 6.53 kg/hr of liquid nitrogen. Exchanger 6 comes after the various hydrogen compressors needed to reach tank storage pressure. This final exchanger lowers the hydrogen down to the required temperature for adsorption. Exchanger 5 requires 4.27 kg/hr liquid nitrogen for its cooling. Both exchangers have no temperature change on the cooling side, as the liquid nitrogen is undergoing a phase change to minimize heat transfer area and cooling mass flows.

The exchangers in Table 3.7.2 provide the cooling for the multi-stage compressions in the process. Exchanger 7 cools the hydrogen as it gets compressed to 30 atm. There are five compressors, so five exchangers are needed. However, since the temperature changes are approximately the same for all five streams, it was decided to pass all five through one exchanger to reduce the infrastructure needed. Exchangers 8 and 9 are for the multi-stage compression of the atmosphere before the pressure swing adsorber at the beginning of the process. The atmospheric compression also requires five compressors. Exchanger 9 covers the first compression, and Exchanger 8 covers the next four compressions. Again, the last four had nearly identical temperature changes, so one exchanger was designed for all four outlets. Cooling in Exchangers 7, 8, and 9 is provided by a 60 wt% ethylene glycol, 40 wt% water solution (i.e. antifreeze). These cooling antifreeze streams feed from Exchanger 7 to Exchanger 8 to Exchanger 9, and are then sent

to Exchanger 10 for recooling. In total, 28.47 kg/hr antifreeze is needed for this process. Exchanger 10 uses liquid hydrogen to recool the antifreeze stream, and again involves vaporization to minimize nitrogen mass flows. This recooling of the antifreeze requires 16.31 kg/hr of liquid nitrogen.

Table 3.7.1. Heat Exchangers in the Mars ISRU Process

HX #	Stream	Inlet Temp (°C)	Outlet Temp (°C)	MoC	Duty (W)	Length (m)	Heat Transfer Area (m^2)
1	**Reducer Inlet**	200	690	Ni Alloy	1079	1.00	0.55
	Cathode Outlet	850	250				
2	**Salts/H_2O (solid to liquid)**	-60	20	Ni Alloy	534	1.16	0.10
	O_2 (gas)	850	144				
3	**Membrane Inlet**	100	224	Ni Alloy	409	1.00	0.15
	Hydrogen Outlet	450	110				
4	**Water Vapor**	115	250	Ni Alloy	258	0.25	0.18
	Membrane Outlet	450	299				
5	**LN_2**	-196	-196	Al	351	0.50	0.08
	O_2 (gas to liquid)	144	-195				
6	**LN_2**	-196	-196	Al	236	0.10	< 0.01
	H_2 (compressed)	0	-195				

Note: The Ni alloy material is composed of a 64 wt% nickel-16 wt% chromium-4 wt% tungsten- 16 wt% molybdenum alloy and has a density of 8.97 g/cm^3 (Haynes Intl., 2015). The outer wall thickness is 1 cm and the inner pipe thickness is 0.5 cm for each heat exchanger.

Table 3.7.2. Heat Exchangers for Compression in the Mars ISRU Process

HX #	Cooling Stream	Inlet Temp (°C)	Outlet Temp (°C)	MoC	Duty (W)	Length (m)	Heat Transfer Area (m^2)
7	**Glycol/Water**	-40	-10	Al	744	1.00	0.23
	H_2 Compression	223	0				
8	**Glycol/Water**	-10	-5	Al	117	1.00	0.10
	Atmospheric Compression 1	96	0				
9	**Glycol/Water**	-5	-4	Al	6	0.25	0.06
	Atmospheric Compression 2	23	0				
10	**LN_2**	-196	-196	Al	905	0.10	0.01
	Glycol/Water	-4	-40				

3.8 Liquid Nitrogen Recycle System

Rationale

Multiple stages of our process require liquid nitrogen (LN_2) for cooling. These processes take liquid nitrogen at 1 atm and -196 ℃ (77 K) and vaporize it. In order to reuse this cooling fluid, a nitrogen recycle system is required that will liquify the nitrogen back. This recycle system allows us to bring liquid nitrogen up to Mars on the initial trip during construction without the need for resupplies throughout the process's lifetime. Without literature to design our own system, we searched through various proprietary systems funded by NASA and selected one for a basis.

Selected System

The proprietary system selected for the liquid nitrogen recycle system is a cryocooler unit developed by Creare, Inc., shown in Figure 3.8.1, awarded a contract by NASA. The working fluid is neon, which flows at 2 atm with a nominal flow rate of 2 g/s (7.2 kg/hr). Based on their 18 kg design, the unit's cooling capacity is 20 W at a load temperature of 77 K. We used this sizing to scale the Creare unit to our liquid nitrogen demand of this Mars ISRU project (Plachta, 2017). Any rejected heat (Q_{rej}) is sent to the biome for heating (heat integration) rather than disposal to the atmosphere or regolith.

Sizing & Scaling

Liquid nitrogen is used in six different places in this process: the glycol/water heat exchanger, the oxygen heat exchanger, the hydrogen heat exchanger, the oxygen tank, the hydrogen tanks, and the dehumidifier heat exchanger. The liquid nitrogen requirements for each unit are given in Table 3.8.1. These calculations assumed the complete vaporization of liquid nitrogen. This allows us to use the minimal amount of liquid nitrogen needed, as merely heating the liquid

nitrogen would require far more cooling fluid. The calculations of these demands are covered in more detail in their respective sections: *Heat Exchangers*, *Tanks*, and *Dehumidifier*.

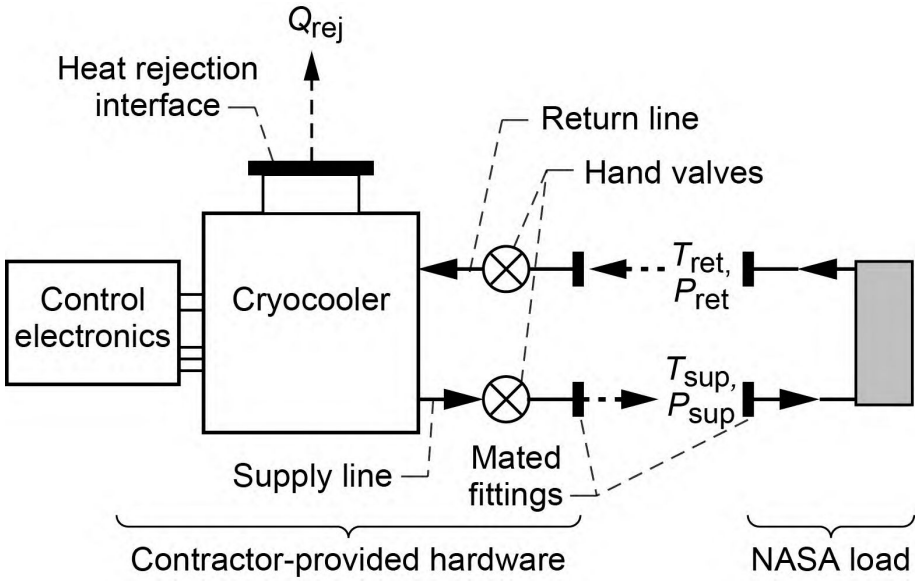

Figure 3.8.1. Schematic of the Creare cryocooler unit. Q_{rej} is the heat load at the rejection interface; P_{sup}, T_{sup}, P_{ret}, and T_{ret} are pressures and temperatures at the supply and return (Plachta, 2017).

Table 3.8.1. LN_2 Requirements for Cryogenic Cooling

Unit	**Heat Duty (W)**	**LN_2 Flow Rate (kg/hr)**
Glycol/Water HX (HX 10)	905	16.31
O_2 HX (HX 5)	351	6.35
H_2 HX (HX 6)	236	4.27
O_2 Tank	4	0.07
H_2 Tank	1,362	24.63
Dehumidifier HX	1,038	18.79
Total Demand	3,896	70.42

The Creare unit was scaled for the 3,896 W cooling demand based on 20 W cooling per 18 kg (Plachta, 2017). It was recommended by our advisor to use a 0.6 scaling factor to account for efficiency improvements and volume differences that come with scale up. The power requirements were scaled based on 17 W per 1 W cooling (Plachta, 2017), which results in a power requirement of 66.23 kWe for the unit. The mass of neon required was assumed to be a matter of the Creare design team, and negligible compared to the mass of the unit for cost purposes. We set the total mass of liquid nitrogen to 70.42 kg to allow us an hour's worth of material in the process.

3.9 Compressors and Pumps

Design Considerations

Compressors in our system were modeled using Aspen. We used the NRTL-HOC property method to match the other NRTL Aspen simulations but to better predict our vapor properties. We assumed 70% mechanical efficiency, as recommended by heuristics (Peters et al., 2003), and used isentropic compressors in all cases. In the cases of our multi-unit compressors, Aspen found the efficiencies to be 72%. Once the simulations were completed, we looked for compressor models that met our demands. We chose rotary compressors from Quincy Compressor as a basis for weight and size (Quincy Compressor, 2012). The hydrogen pumps, however, were selected following reciprocating L&W compressors, as they are tailored to hydrogen compression and provide more versatility in pressure changes and power options (L&W Compressors, n.d.). The material of construction is predominantly steel, and weights are given in specification sheets.

Pumps were also simulated in Aspen. Again, we used the NRTL method for our fluid properties, and assumed a 70% mechanical efficiency. We then found models for products that we could use as a basis in our process. Gorman-Rupp provided models for the use of water transportation (Gorman-Rupp, n.d.), and Graco had suitable models for antifreeze transport (Graco, n.d.).

Mid-process Compressors

Within our process, there are two compressors meant to maintain needed pressures for our unit operations, as well as to preheat the streams before they enter the unit operations. The first compressor handles the reducer cathode outlet stream before it enters the WGS reactor. This compressor uses 35 W to compress the outlet stream from 0.86 atm to 1 atm, and increases the

stream temperature to 137 ℃. For this purpose, we selected the Quincy QGS5 compressor to provide the needed power (Quincy Compressor, 2012). The second compressor repressurizes the dehumidifier system's outlet stream before it enters the membrane hydrogen separator. The dehumidifier outlet stream leaves at 1.00 atm, and needs to be compressed to 1.50 atm for the operation of the membrane. The compressor simulation gave a compressor that requires 263 W of power to reach 1.50 atm and 288 ℃. We chose to use another Quincy QGS5 compressor for this compression (Quincy Compressor, 2012).

Multi-unit Compressors

To compress the atmosphere to the desired operating pressure of 1 atm, we designed a series of five compressors to reach 1 atm from the ambient 0.006 atm. An Aspen simulation was set up to design the compressors with equivalent compression ratios. It also requires a cooling system between compressions to maintain the correct inlet temperature for the pressure swing adsorber. The total work of the system is 40 W and the total cooling is 36 W. The compressors consist of five Quincy compressors separated by the cooling units (Quincy Compressor, 2012). See the *Heat Exchanger* section for the cooling design.

A five compressor system is required to compress the hydrogen before it enters our tanks. These compressors take the gas from the membrane outlet of 1 atm to 30 atm for proper storage. This system requires 616 W of total work and 746 W of total cooling. Again, see the *Heat Exchanger* section for the cooling design. The five compressors are all L&W hydrogen compressors, as mentioned earlier (L&W Compressors, n.d.).

Pressure Swing Compressors

As part of our process, we have two sets of two pressure swing adsorber columns to purify some of our vapor streams. The first set of columns captures CO_2 from the atmosphere and separates it from the N_2 and Ar present. The column designs are detailed further in the *Atmospheric Compression* section. It follows the atmospheric multi-unit compression system mentioned above. The second pressure swing columns are the desiccant columns, detailed in the *Dehumidifier* section, completing the water removal process.

One compressor compresses the gas in both columns for atmospheric capture. This compressor, based on our simulations, requires 29 W of power, and causes the outlet temperature to reach 230.65 ℃. Following our other compressor designs, this compressor is a Quincy QGS5 compressor in order to meet the power demands (Quincy Compressor, 2012).

The desiccant columns have pressure swing components in order to remove the water from the WGS outlet. The sieve, at 107 ℃, only requires a pressure of 1 atm to complete adsorption. The stream leaves the WGS at 0.86 atm. Aspen simulations yielded a compression work of 227 W and an outlet temperature of 280 ℃. A Quincy QGS5 compressor is used for these purposes.

Process Pumps

The evaporator has two feed streams: the incoming brine feed and the dehumidifier recycle. The evaporator operates at 1 atm. Because of this, both streams are pressurized to 1.5 atm to account for frictional pressure losses through pipes and unit operations. The pump for the liquid brine has a work duty of less than 1 W and an outlet temperature of 20 ℃. The pump for the liquid water recycle stream has a work duty of less than 1 W and an outlet temperature of 70 ℃. These

pumps are both Gorman-Rupp O-Series pumps. We selected aluminum pumps with a maximum of 1 hp of power (Gorman-Rupp, n.d.).

The antifreeze pump handles our glycol/water movement in the process. Antifreeze enters three heat exchangers at -40 °C and 2.96 atm and exits the final exchanger at 0 °C and 0.97 atm. Our pump repressurizes the stream to 2.96 atm, and then we cool the stream back down to -40 °C using a liquid nitrogen recycle system (see the *Heat Exchangers* section). This pump also requires little work, so a Graco 3/4 hp pump is used for these purposes.

While we do have liquid nitrogen in the process, we did not design a pump for this process. This is because of the proprietary recycling system mentioned in the *Liquid Nitrogen Recycle* section. Since the Creare design covers the recycling and processing of the nitrogen, the pumping is included in that design (Plachta, 2017).

3.10 Tanks

Tanks Overview

Throughout the operation of the current process, storage tanks are needed to hold the produced hydrogen gas and liquid oxygen, to provide intermediary stations for CO_2 and liquid nitrogen in the process, and to hold the glycol/water solution that had to be shipped from Earth since it is not refined on Mars. These storage tanks are subject to the temperature and weather conditions of the Martian atmosphere, and therefore the thicknesses of the material of construction and insulation must be considered in order to sustain the pressure and temperature differentials. There are six separate compounds that would need storage tanks in this process: gaseous carbon dioxide, gaseous hydrogen, liquid oxygen, liquid nitrogen, glycol/ water, and gaseous inert atmospheric components. A summary of the design parameters of each storage tank is found in Tables 3.10.1 and 3.10.2.

The dimensions of each tank were calculated based on the total flow rate into it and the storage duration of its contents. The CO_2, liquid nitrogen, and glycol/water tanks are assumed to be 10-minute holding tanks because they are used for short-term storage, while the inert storage tank is assumed to be a 1-hour holding tank due to its less frequent use for regeneration of the molecular sieve in the dehumidifier. Each tank is made of aluminum due to its compatibility with the stored fluids and its thermal stability at the maintained tank temperatures. Design for the thickness of each of the tanks was determined through Barlow's formula (Eqn. 3.10.1) (Legal Information Institute, n.d.).

Equation 3.10.1: $$t = \frac{Pd}{2SEF - P}$$

In the formula, t is the thickness of the tank wall in millimeters; P is the internal pressure in kPa gauge; d is the inner diameter of the wall; S is the yield strength, which is 276,000 kPa for all cases using aluminum; E is the seam joint factor, which is equal to unity since all tanks are nearly seamless; and F is the design factor, which is typically 0.72 (Legal Information Institute, n.d.). In many cases the thickness of the tank wall was calculated to only be a few millimeters; those thicknesses were rounded up to 1 cm in order to sustain Martian atmospheric conditions.

Additionally the energy required to maintain the temperature of each of the tanks was calculated using the heat transfer formula from Wankat (Eqn. 3.10.2) across the aluminum wall and 37 layers of multilayer insulation (MLI) according to Ross (2015). An ambient temperature of -60°C was assumed, based on the average atmospheric temperature of Mars (Sharp, 2017).

Equation 3.10.2: $$q = \frac{\Delta T * S.A.}{\frac{37}{0.025} + \frac{0.01}{229}}$$

Equation 3.10.3: $$S.A. = 2\pi r_i (L + r_i)$$

In Equation 3.10.2, q is the heat transfer in Watts, ΔT is the difference between the stored material temperature in Kelvin and ambient temperature (213 K), S.A. is the surface area of the inside of the tank in m^2, 37 refers to the number of MLI layers, 0.025 refers to the conductivity coefficient of MLI in mW/m^2K, 0.01 is the thickness of the aluminum in meters, and 229 is the conductivity coefficient of aluminum. To calculate the inside surface area of the tank, Eqn. 3.10.3 uses r_i which is the inside radius of the tank, and L which is the length of the tank.

Hydrogen Tank Details

In order to maximize the amount of hydrogen that can be stored, we decided to adsorb the hydrogen onto a graphene mesh inside the hydrogen tank. Based on an assumed 10 wt% hydrogen per wt% graphene, a required mesh volume of 39.6 m^3 was determined (Baburin et al., 2015). A

horizontal tank with a length equal to double the width was assumed to calculate the dimensions. An aluminum tank wall was used as the basis for the mass calculation. The thickness and energy requirements of the hydrogen tank were calculated in the same way as those of the other tanks, as described above. The hydrogen tank dimensions and further details can be seen in Tables 3.10.1 and 3.10.2.

Table 3.10.1. Mass Flow Rates into Process Storage Tanks and their Dimensions

I.D.	Stored Fluid	Mass Flow Rate (kg/hr)	Volume (m^3)	Length (m)	Diameter (m)
TK-1	**CO_2**	6.749	5.063	1.62	0.81
TK-2	**(2 tanks) H_2**	0.300	(total) 39.560	4.66	2.33
TK-3	**O_2**	2.385	23.660	3.11	3.11
TK-4	**LN_2**	70.420	0.014	0.26	0.26
TK-5	**Glycol/Water**	29.020	0.004	0.28	0.14
TK-6	**Inerts**	< 0.001	0.001	0.39	0.19

Table 3.10.2. Storage Conditions, Materials of Construction, Wall Thicknesses, and Energy Requirements of Process Storage Tanks

I.D.	Stored Fluid	Temperature (℃)	Pressure (atm)	Material of Construction	Thickness of Tank Walls (cm)	Energy Requirement due to Heat Loss (W)
TK-1	**CO_2**	125	1	Al	1	0.644
TK-2	**(2 tanks) H_2**	-197	30	Al	2	7.894
TK-3	**O_2**	-197	1	Al	1	4.219
TK-4	**LN_2**	-197	1	Al	1	0.029
TK-5	**Glycol/Water**	-40	3	Al	1	0.002
TK-6	**Inerts**	0	1	Al	1	0.004

3.11 Power

This process is powered by NASA's Kilopower technology. Kilopower is a near-term technology that is currently in development by NASA to be an affordable fission nuclear power system. This power system was selected for the process because it is designed to enable long-duration stays on planetary surfaces that require ISRU, especially on the Moon and Mars. It is also resistant to environmental hazards, particularly Martian dust storms, which would compromise generation of solar power (Hall, 2017).

Kilopower comes in two designs for 1-3 kWe and 3-10 kWe power requirements. This process uses the 10 kWe version for operation on the Martian surface (NASA, 2018). Its setup can be viewed in Figure 3.11.1. As stated in the *Economics* section, the total power demand is 93 kW, so ten Kilopower units are required for this process.

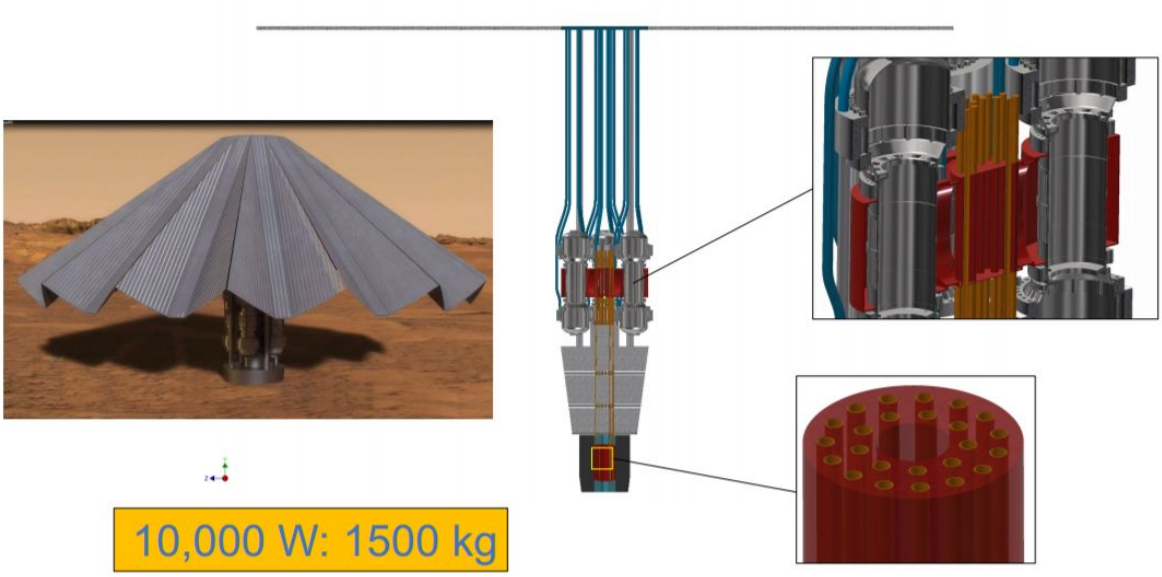

Figure 3.11.1. 3-10 kWe Surface Concept Version of Kilopower (NASA, 2018)

A specific type of Kilopower reactor is KRUSTY, the Kilopower Reactor Using Stirling TechnologY (see Figure 3.11.2). Using KRUSTY, NASA has demonstrated that it is possible to run a passive reactor operation of the Kilopower reactor class between 1 and 10 kWe. By utilizing the Stirling engine design, KRUSTY can passively handle any possible state of the power-conversion system by drawing more or less power, thereby accommodating worst-case failures (NASA, 2018). As NASA continues to develop its Kilopower reactors, the best designs will be selected for future Mars missions.

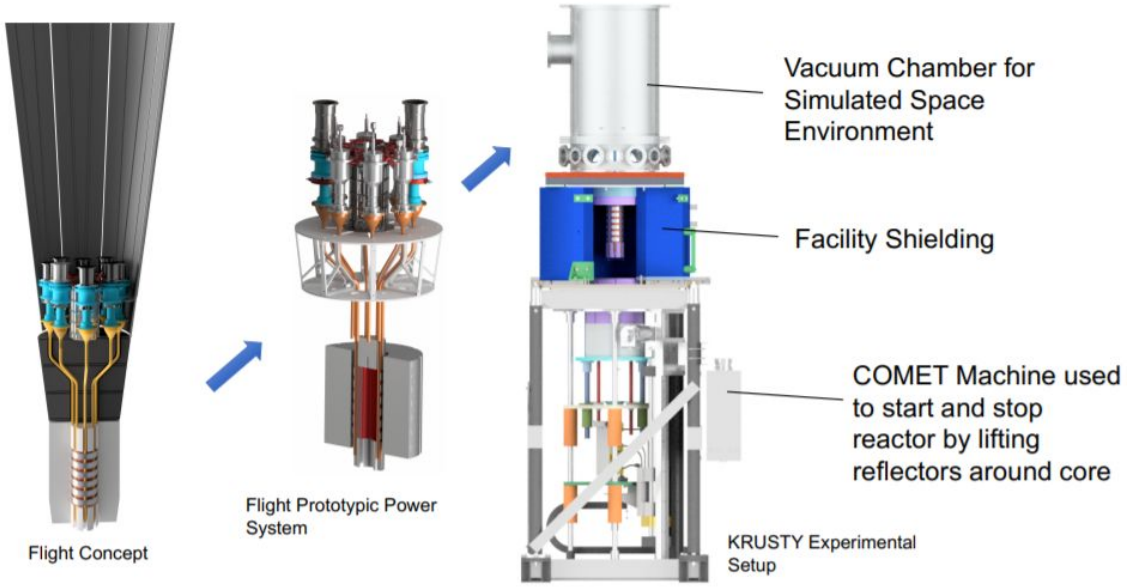

Figure 3.11.2. KRUSTY Design (NASA, 2018)

4. Final Process Design

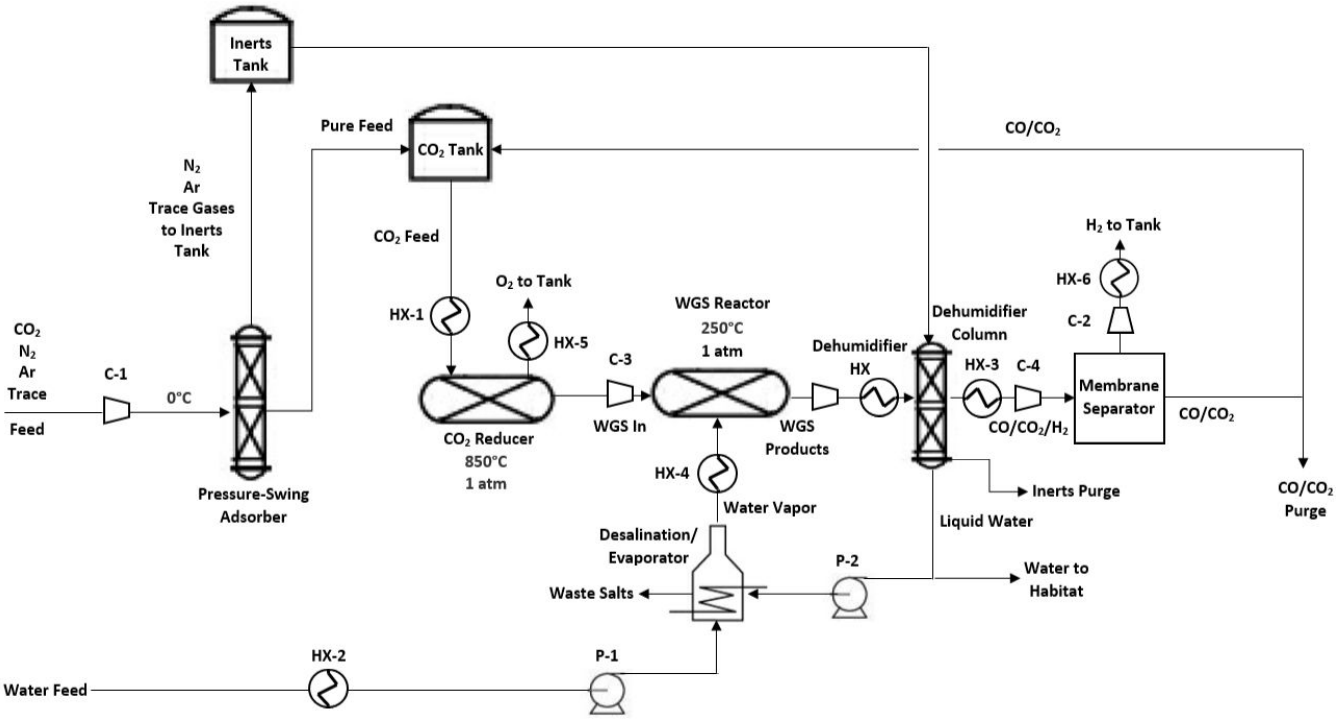

Figure 4.0.1. Process flow diagram of the Mars ISRU process.

Table 4.0.1. Overall Process Stream Table of CO/CO_2 Purge, CO_2 Feed, CO_2 Recycle, and Reducer Inlet Streams

Streams	CO/CO_2 Purge	CO_2 Feed	CO_2 Recycle	Reducer Inlet
Phase	Vapor	Vapor	Vapor	Vapor
Temperature (°C)	80	125	80	850
Pressure (atm)	1	1	1	1
H_2 (kg/hr)	0	0	0	0
CO (kg/hr)	< 0.01	< 0.01	0.12	0.12
O_2 (kg/hr)	0	0	0	0
CO_2 (kg/hr)	0.33	0.34	6.29	6.63
H_2O (kg/hr)	0	0	0	0

Table 4.0.2. Overall Process Stream Table of O_2 Product, WGS Inlet, and WGS Product Streams

Streams	O_2 Product	WGS Inlet from Reducer	WGS H_2O Inlet	WGS Products to Dehumidifier
Phase	Vapor	Vapor	Vapor	Vapor
Temperature (°C)	850	250	115 to 250	255 to 107
Pressure (atm)	1	1	1	0.86 to 1
H_2 (kg/hr)	0	0	0	0.30
CO (kg/hr)	0	4.30	0	0.13
O_2 (kg/hr)	2.38	0	0	0
CO_2 (kg/hr)	0	0.07	0	6.63
H_2O (kg/hr)	0	0	8.21	5.53

Table 4.0.3. Overall Process Stream Table of H_2O Recycle, Habitat, and Feed, Membrane, and H_2 Product Streams.

Streams	H_2O Recycle	H_2O to Habitat	H_2O Feed	Membrane Inlet	Membrane Outlet	H_2 Product Purge
Phase	Liquid	Liquid	Liquid	Vapor	Vapor	Vapor
Temperature (ºC)	70	70	20	80 to 450	450	450
Pressure (atm)	1	1	1	1.0 to 1.5	1.5	1.0
H_2 (kg/hr)	0	0	0	0.30	0	0.30
CO (kg/hr)	0	0	0	0.13	0.13	0
O_2 (kg/hr)	0	0	0	0	0	0
CO_2 (kg/hr)	0	0	0	6.63	6.63	0
H_2O (kg/hr)	4.59	0.94	3.62	0	0	0

Table 4.0.4. Overall Process Stream Table of Inerts and Salts

Streams	Atmospheric Feed	Dehumidifier	Evaporator
N_2 (kg/hr)	0.011	0.011	0
Ar (kg/hr)	0.007	0.007	0
Waste Salts (kg/hr)	0	0	0.77

4.1 Atmospheric Pressure-Swing Adsorber

The atmospheric pressure-swing adsorber separates carbon dioxide from other inert gases that are retrieved from the atmosphere, and compresses the gas to the desired system pressure. A stream table of the adsorber can be seen in Table 4.1.1 below.

Table 4.1.1. Atmospheric Compression Stream Table

Component (kg/hr)	**Atmospheric Feed (0 ºC, 1 atm)**	**Inert Stream (231 ºC, 1 atm)**	**CO_2 Stream (231 ºC , 1 atm)**
N_2	0.011	0.011	0.000
Ar	0.007	0.007	0.000
CO	0.001	0.000	0.001
CO_2	0.340	0.000	0.340

Gases from the atmosphere are pumped into the column at 1 atm and pressurized to 10 atm to reach breakthrough, which is the separation of the inert gases. Afterwards, the column is depressurized to 1 atm. Each column is packed with 1.87 kg aluminum-silica-sodia sorbent and has dimensions of 0.18 m length and 0.06 m diameter. The column requires 29 W of power and raises the outlet stream temperatures to 231 °C.

4.2 Carbon Dioxide Reducer

The carbon dioxide reducer is the main means of producing oxygen in our process. It is an electrochemical reactor that reduces carbon dioxide into carbon monoxide and oxygen. The oxygen is stored as oxidizer or sent to the human habitat and the carbon monoxide is sent to the WGS reactor to aid in hydrogen production. A stream table of the reducer can be seen in Table 4.2.1 below.

Table 4.2.1. Carbon Dioxide Reducer Stream Table

Component (kg/hr)	**Reducer Inlet (850 ºC, 1 atm)**	**Cathode Outlet (850 ºC, 0.86 atm)**	**Anode Outlet (850 ºC, 0.86 atm)**
O_2	0.00	0.00	2.38
CO	0.12	4.30	0.00
CO_2	6.63	0.07	0.00

The reactor consists of 954 kg of catalyst that is predominantly a yttria-stabilized zirconia (YSZ) catalyst, with nickel (Ni) additives in the cathode and Lanthanum Strontium Manganite (LSM) additives in the anode. The reactor runs at 850 °C and has a pressure drop of 0.16 atm due to the catalyst packing. The reactor is 0.5 m long and 0.9 m in diameter to achieve the necessary conversion and heat transfer.

4.3 Water Evaporation/Desalination Unit

The water evaporation and desalination unit fully separates the Martian salts from the inlet water feed, and vaporizes the feed and recycle water streams. The waste salts are discarded onto the Martian surface. A stream table of the unit can be seen in Table 4.3.1 below.

Table 4.3.1. Evaporation/Desalination Unit Stream Table

Component (kg/hr)	**Brine Feed (20 °C, 1.5 atm)**	**Water Recycle Feed (70 °C, 1 atm)**	**Waste Salts (115 °C, 1 atm)**	**Water Vapor Outlet (115 °C, 1 atm)**
H_2O	3.62	4.59	0.00	8.21
Salts	0.77	0.00	0.77	0.00

The inlet brine mixture is at 20 °C and 1.5 atm and the water recycle stream is at 70 °C and 1 atm. The evaporation/desalination unit is operated at 115 °C and 1 atm, is 0.3 m in diameter and 0.6 m in height, and is constructed from NASA-427 aluminum alloy. A 45 L capacity, electric BriskHeat copper heating jacket is used to heat the unit, which requires 5.2 kW of power.

4.4 Water-Gas Shift Reactor

The WGS reactor uses a CuO catalyst (ICI Catalyst 52-1) to produce the desired H_2 product. The unit is a 0.2 m long, 0.2-m diameter plug flow (packed bed) reactor made of titanium. The total mass of the reactor is 21 kg, which includes both the weight of the titanium walls (2.7 kg) and of the catalyst packing (18.3 kg). A stream table of the WGS reactor can be seen in Table 4.4.1 below.

Table 4.4.1. Water-Gas Shift Reactor Stream Table

Component (kg/hr)	**WGS Feed (250 °C, 1 atm)**	**H_2O Inlet (115 °C, 1 atm)**	**WGS Products (255 °C, 0.87 atm)**
H_2	0.00	0.00	0.30
CO	4.30	0.00	0.13
CO_2	0.07	0.00	6.63
H_2O	0.00	8.21	5.53

Operation of the WGS reactor is at 1 atm and the gaseous mixture of CO_2, CO, and water vapor is preheated to 250 °C prior to entering the reactor. The reactor runs excess water to increase the conversion of CO, which increases the production of H_2. It is necessary to produce excess hydrogen fuel in addition to oxygen because liquid oxygen/liquid hydrogen rockets perform best when fuel rich (Braeunig, 2012). This unit requires 40 W of cooling duty.

4.5 Dehumidifier

The dehumidifier is a series of units that removes water from the WGS outlet stream before it enters the membrane separator. The recovered water is either recycled back into the evaporator or sent to the human habitat. A stream table of the dehumidifier can be seen in Table 4.5.1 below.

Table 4.5.1. Dehumidifier Stream Table

Component (kg/hr)	Inlet (107 °C, 1 atm)	Water Recycle (70 °C, 1 atm)	Water to Habitat (70 °C, 1 atm)	Membrane Feed (80 °C, 1 atm)
H_2	0.30	0.00	0.00	0.30
CO	0.13	0.00	0.00	0.13
CO_2	6.63	0.00	0.00	6.63
H_2O	5.53	4.59	0.94	0.00

Table 4.5.2. Inerts Stream Table

Component	Flow Rate (kg/hr)
N_2	0.011
Ar	0.007
H_2O*	< 0.01

**Water loss due to regeneration negligible.*

Note: Inlet and outlet flow rates remain constant because the inerts are not consumed or separated.

First, the WGS outlet is compressed to 1 atm, which raises the stream temperature to 280°C. This compressor requires 227 W of power for the necessary temperature change. The stream is then cooled to 107 °C using a liquid nitrogen-cooled heat exchanger. This heat exchanger is 0.1 m long with a heat transfer area of 0.01 m^2, and made of Ni-alloy to withstand the hot stream temperatures.

The streams then enter a series of desiccant pressure-swing adsorption columns. Each column is packed with 0.31 kg of Zeolite 3A to cover an hour's worth of incoming water vapor. Each column is 0.18 m long and 0.06 m in diameter. The inert gases removed from the atmospheric separation are used to regenerate the zeolite.

4.6 Membrane Separator

The palladium membrane inside the piping that leads to the CO/CO_2 purge valve separates hydrogen from the CO, CO_2, and H_2 dehumidifier outlet stream. A stream table of the membrane can be seen in Table 4.6.1 below.

Table 4.6.1. Membrane Stream Table

Component (kg/hr)	Membrane Feed (450 °C, 1.5 atm)	H_2 Permeate (450 °C, 1.0 atm)	CO/CO_2 Recycle (450 °C, 1.5 atm)	CO/CO_2 Purge (110 °C, 1.0 atm)
H_2*	0.30	0.30	0.00	0.00
CO	0.13	0.00	0.12	0.01
CO_2	6.63	0.00	6.30	0.33

** A small amount of hydrogen will likely remain in the retentate.*

The coating on a stainless steel support tube is a 93 wt% palladium and 7 wt% yttrium alloy to prevent side reactions on the membrane surface. Dimensions of the support tube are 0.3 m thickness and 0.1 m length. The thickness of the alloy coating is 13 μm. To achieve full hydrogen separation, the membrane has a pressure drop from 1.5 atm to 0.5 atm for the permeate stream, while the retentate stream remains at 1.5 atm. The retentate stream is then depressurized by the CO/CO_2 purge to 1 atm. To prevent CO degradation of the membrane, the membrane inlet stream is heated from 288 °C to 450 °C with a 1.5 kW IJ-G electric heating jacket from ElectroHeat.

4.7 Compressors and Pumps

The compressors in our system help maintain operating conditions and storage of important gases in our process. The pumps help maintain fluid flow amongst various unit operations. All compressor and pump calculations were run in Aspen, which provided energy demands and sizing requirements based on volumetric flow rates. As seen in Table 4.7.1, all of the compressors and pumps are listed with their given design basis type (quantity in parentheses), pressure change, power requirement, and mass for shipping. Specifics and reasons for use of the Quincy and L&W compressors can be seen in the *Compressors and Pumps* section.

Table 4.7.1. Design Specifications of the Compressors and Pumps in the Process

I.D.	Compressors & Pumps	Type	Pressure Change (atm)	Power (kW)	Mass (kg)
	Compressors				**1,855**
C-1	Atmospheric Range	Quincy (5)	0.99	0.076	550
C-2	H_2 Range	L&W (5)	29.00	1.362	975
C-3	WGS Inlet	Quincy	0.14	0.035	110
C-4	Membrane Inlet	Quincy	0.50	0.361	110
C-5	CO_2 Pressure-Swing	Quincy	9.00	0.029	55
C-6	Desiccant Pressure-Swing	Quincy	0.14	0.227	55
	Pumps				**129**
P-1	Water (Liquid Brine)	Gorman-Rupp	0.5	< 0.001	45
P-2	Water (Recycle)	Gorman-Rupp	0.5	< 0.001	45
P-3	Glycol/Water System	Graco (1)	1.5	0.905	39

4.8 Tanks

Each tank was designed according to the total inlet volumetric flow rate as well as the holding time of the material in the tank. The tank specifications can be seen in Tables 4.8.1 - 4.8.3. Aluminum was used as the material of construction for the tanks because none of the tanks are at temperatures high enough to reduce the performance of aluminum. The tanks are insulated with 37 layers of aluminized mylar multilayer insulation, which greatly reduces the loss of heat from the tanks.

Table 4.8.1. Functions of the Storage Tanks

CO_2 tank	● 10-minute holding tank ● Collects atmospheric compression and membrane recycle streams before they enter the reducer cathode
Two H_2 tanks	● Stores H_2 product from the WGS reactor ● Adsorbed to a graphene mesh
O_2 tank	● Stores O_2 product from the CO_2 reducer
Liquid N_2 tank	● 10-minute holding tank before cooling applications
Glycol/Water tank	● 10-minute holding tank before cooling applications
Inert tank	● 1-hour holding tank ● Collects atmospheric inerts (i.e. Ar and N_2) before desiccant column regeneration

Table 4.8.2. Design Specifications of Storage Tanks

I.D.	Stored Fluid	Mass Flow Rate (kg/hr)	Volume (m^3)	Length (m)	Diameter (m)
TK-1	**CO_2**	6.749	5.063	1.62	0.81
TK-2	**(2 tanks) H_2**	0.300	(total) 39.560	4.66	2.33
TK-3	**O_2**	2.385	23.660	3.11	3.11
TK-4	**LN_2**	70.420	0.014	0.26	0.26
TK-5	**Glycol/Water**	29.020	0.004	0.28	0.14
TK-6	**Inerts**	< 0.001	0.001	0.39	0.19

Table 4.8.3. Additional Design Specifications of Storage Tanks and Heat Loss

I.D.	Stored Fluid	Temperature (℃)	Pressure (atm)	Material of Construction	Thickness of Tank Walls[3] (cm)	Energy Requirement Due to Heat Loss[2] (W)
TK-1	**CO_2**	125	1	Al	1	0.644
TK-2	**(2 tanks) H_2**	-197	30	Al	2	7.894
TK-3	**O_2**	-197	*1	Al	1	4.219
TK-4	**LN_2**	-197	1	Al	1	0.029
TK-5	**Glycol/Water**	-40	3	Al	1	0.002
TK-6	**Inerts**	0	1	Al	1	0.004

***** *Assumed minimal pressure drop in the anode of the reducer.*

4.9 Power

Electrical power in our process is provided by Kilopower units developed by NASA. The units use nuclear and solar energy to produce 10 kWe each. The systems are self contained, so little maintenance is needed on them. Our process requires ten Kilopower units to run.

5. Process Economics

5.1 Mass Costs

The primary cost associated with our process is the mass transported to Mars. The masses of the unit operations, heat exchangers, compressors, pumps, tanks, and consumables used can be seen in Tables 5.1.1 - 5.1.5 below. In addition to these, a total piping mass of 910.2 kg is required. The piping mass was calculated through a rough estimation of material of construction volumes. The materials of construction were estimated as stainless steel around the evaporator, titanium and nickel-aluminum alloy around the CO_2 reducer, titanium for the WGS reactor, and aluminum for everything else. The mass may actually exceed 1200 kg, since we assumed the length of all the pipes to be a meter; realistically these pipes may be longer, especially for the recycle streams. The total mass of the equipment, consumables, kilopower units, liquid nitrogen recycle system, and piping is 50,043 kg. The majority of the mass requirement (76 %) is from the YSZ catalyst for the CO_2 reducer (46 %) and Kilopower units (30 %). Based on the assumption that every kilogram of material launched from Earth costs $22,026, a total shipping cost of $1,102,247,118 is necessary (NASA, 2008).

Table 5.1.1. Masses of the Unit Operations in the Process

Unit Operation	Mass (kg)
CO_2 Reducer	1,134
Reducer Heating Jacket*	550
H_2 Separation Membrane*	110
Desalination/Evaporator Heating Jacket	27
Desalination/Evaporator	24
Water Gas Shift Reactor	21
Pressure Swing Adsorber (2)	(total) 7
Dehumidifier Flash Heating Jacket	4
Dehumidifier Sieves (2)	(total) 2
Kilopower Unit (10)**	15,000
LN_2 Recycle System (Creare)	426

** ElectroHeat carrier assembly mass is not included, as it is proprietary.*

*** Based on a 1,500 kg mass of each Kilopower unit (McClure, 2019)*

Table 5.1.2. - Masses of the Heat Exchangers in the Process

I.D.	Location	Outer Shell (kg)	Inner Pipes (kg)	Total Mass (kg)
HX-1	**Reducer Inlet - Cathode Outlet**	138	30	168
HX-2	**Salts/H_2O - O_2 (gas)**	36	6	42
HX-3	**Membrane Inlet - Hydrogen Outlet**	88	20	108
HX-4	**Water Recycle - Membrane Outlet**	21	1	22
HX-5	**LN_2 - O_2**	3	1	4
HX-6	**LN_2 - H_2**	1	0.5	1.5
HX-7	**Glycol/Water - H_2 Compression**	16	18	34
HX-8	**Glycol/Water - Atmospheric Compression 1**	6	6	12
HX-9	**Glycol/Water - Atmospheric Compression 2**	1	0.5	1.5
HX-10	**LN_2 - Glycol/Water**	1	0.5	1.5

Table 5.1.3. Masses of the Compressors and Pumps in the Process

I.D.	Unit	Mass (kg)
	Compressors	
C-1	Atmospheric Range (Quincy) (5)	550
C-2	H_2 Range (L&W) (5)	975
C-3	WGS Inlet (Quincy)	110
C-4	Membrane Inlet (Quincy)	110
C-5	CO_2 Pressure-Swing (Quincy)	55
C-6	Desiccant Pressure-Swing (Quincy)	55
	Total	1,855
	Pumps	
P-1	Water (Gorman-Rupp) (2)	90
P-2	Glycol/Water (Graco) (1)	39
	Total	129

Table 5.1.4. Masses of the Tanks in the Process

I.D.	Unit	Mass (kg)
TK-1	**CO_2**	142
TK-2	**H_2 (2)**	(total) 4,669
TK-3	**O_2**	1,239
TK-4	**LN_2**	9
TK-5	**Glycol/Water**	5
TK-6	**Inerts**	9

Table 5.1.5. Masses of Consumables in the Process

Component	Mass (kg)
YSZ Catalyst (2 beds)	22,896
ICI Catalyst 52-1 (minimum)	216
Zeolite 3A (3 for each column)	24
Alumina Silica Sodia Sorbent (5 for each column)	240

Note: Miscellaneous backup parts are not included and are considered out of scope for the current project.

5.2 Power Costs

The power requirement of each unit operation, compressor, pump, and tank is seen in Tables 5.2.1 and 5.2.2 below. The total power requirement of 93 kW is satisfied through the use of ten 10 kWe Kilopower units, resulting in a total power cost of $200,000,000 (Hall, 2017; Nikolewski, 2018).

Table 5.2.1. Unit Operation Energy Flows in the Process

Unit Operation	Power Requirement (kW)
CO_2 Reducer	12.93
Water Gas Shift Reactor	0.04
Desalination/Evaporator	5.16
Dehumidifier	4.28
Membrane Heating Jacket	1.50
Pressure Swing Adsorber	See *Table 5.3.3*
LN_2 Recycle	66.23
Unit Operations Total*	*90.14*

** Does not include the power of the pressure swing adsorber.*

Table 5.2.2. Compressor and Pump Energy Flows in the Process

#	Unit	Power Requirement (kW)
	Compressors	
C-1	Atmospheric Range	0.076
C-2	H_2 Range	1.362
C-3	WGS Inlet	0.035
C-4	Membrane Inlet	0.361
C-5	CO_2 Pressure Swing	0.029
C-6	Desiccant Pressure-Swing	0.005
	Pumps	
P-1	Liquid Brine	<0.001
P-2	Water Recycle	<0.001
P-3	Glycol/Water System	0.905
	Compressors & Pumps Total	*2.778*

Note: Tanks are not included in the power costs since those that require heating will lose less than one watt of heat and the storage material will be well circulated as they are either 10-minute or 1-hour holding tanks.

5.3 Capital Costs

The bare module costs of the unit operations, heat exchangers, compressors and pumps, and tanks in the process, calculated using CAPCOST with the exception of the membrane separator, can be seen in Tables 5.3.1 - 5.3.4 below (Turton, 2009). Since our process unit capacities are below the minimums of CAPCOST, the minimum bare module costs were scaled based on the CEPCI values of 542 and 596.1 from 2017 and 2019, respectively (Turton, 2009; Economic Indicators, 2020). The cost of the liquid nitrogen recycle system is $749,900 based on the contract that NASA signed with Creare (Creare*,* 2017*)*. Based on these costs, the total bare module equipment cost of the Mars ISRU process, also including the Kilopower units, is $205,226,144. In addition, the cost of piping for the equipment is $10,261,307 based on the assumption that it is 5% of the equipment costs, as recommended by our advisor. Additionally, the total cost of liquid nitrogen and antifreeze used for cooling is $241,857, as seen in Table 5.3.5. The cost of consumables for the process is $3,324,504, based on Table 5.3.6. The amount of replacement consumables was calculated using lifetimes of the catalysts across the lifetime of the factory. Spare parts outside the consumables listed are considered out of scope for the current work.

Table 5.3.1. Process Main Unit Operation Equipment Capital Costs

Unit Operation	Actual Volume (m^3)	Bare Module Volume (m^3)	Bare Module Cost ($)	Scaled Bare Module Cost ($)
CO_2 Reducer	0.417	5	39,200	43,113
Water Gas Shift Reactor	0.004	5	39,200	43,113
Desalination/ Evaporator	0.0424	1	28,100	30,905
Dehumidifier - Flash Drum	0.00196	0.3	10,900	11,988
Dehumidifier - Desiccant Column	5.65×10^{-5}	0.3	18,400	20,237
Membrane *	-	-	-	3,712
Pressure Swing Adsorber	5.089×10^{-4}	0.3	8,510	9,359

** Membrane cost is based on the alloy composition of the powder coating, prices of palladium and yttrium, and a price of $3/lb of stainless steel (Sciencing, 2018; Sigma Aldrich, 2020). The price of the ElectroHeat IJ-G proprietary heater is not included.*

Table 5.3.2. Process Heat Exchanger Capital Costs

I.D.	Heat Exchanger	Actual Heat Transfer Area (m^2)	Bare Module Heat Transfer Area (m^2)	Bare Module Cost ($)	Scaled Bare Module Cost ($)
	Dehumidifier - HX	0.32	1	9,930	10,921
HX-1	**Reducer Inlet - Cathode Outlet**	0.55	1	22,700	24,966
HX-2	**Salts/H_2O - O_2 (gas)**	0.10	1	22,700	24,966
HX-3	**Membrane Inlet - Hydrogen Outlet**	0.38	1	22,700	24,966
HX-4	**Water Vapor - Membrane Outlet**	0.18	1	22,700	24,966
HX-5	**LN_2 - O_2**	0.08	1	9,930	10,921
HX-6	**LN_2 - H_2**	0.01	1	9,930	10,921
HX-7	**Glycol/Water - H_2 Compression**	0.23	10	95,000	104,482
HX-8	**Glycol/Water - Atmospheric Compression 1**	0.10	10	89,300	98,214
HX-9	**Glycol/Water - Atmospheric Compression 2**	0.06	1	9,930	10,921
HX-10	**LN_2 - Glycol/Water**	0.06	1	9,930	10,921

Table 5.3.3. Process Compressor and Pump Capital Costs

I.D.	Compressors & Pumps *	Actual Power (kW)	Bare Module Power (kW)	Bare Module Cost ($)	Scaled Bare Module Cost ($)
	Compressors				
C-1	Atmospheric Range 1 (Quincy)	0.00658	18	39,200	43,113
	Atmospheric Range 2 (Quincy)	0.00834	18	39,200	43,113
	Atmospheric Range 3 (Quincy)	0.00833	18	39,200	43,113
	Atmospheric Range 4 (Quincy)	0.00832	18	39,200	43,113
	Atmospheric Range 5 (Quincy)	0.00828	18	39,200	43,113
C-2	H_2 Range 1 (L&W)	0.137	450	689,000	757,773
	H_2 Range 2 (L&W)	0.130	450	689,000	757,773
	H_2 Range 3 (L&W)	0.123	450	689,000	757,773
	H_2 Range 4 (L&W)	0.116	450	689,000	757,773
	H_2 Range 5 (L&W)	0.110	450	689,000	757,773
C-3	WGS Inlet (Quincy)	0.035	18	39,200	43,113
C-4	Membrane Inlet (Quincy)	0.361	18	39,200	43,113
C-5	CO_2 Pressure-Swing (Quincy)	0.0289	18	39,200	43,113
C-6	Desiccant Pressure-Swing (Quincy)	0.227	18	39,200	43,113
	Pumps				
P-1, P-2	Water (Gorman-Rupp) (2)	0.00016	1	21,600	23,756
P-3	Glycol/Water (Graco)	0.5593	1	15,500	17,047

** Since the material for the rotary Quincy compressors is unlisted, it is assumed that they have a material cost factor equal to that of carbon steel. The reciprocating L&W compressors are assumed to be made of stainless steel.*

Table 5.3.4. Process Tank Capital Costs

I.D.	Tank	Actual Volume (m^3)	Bare Module Volume (m^3)	Bare Module Cost ($)	Scaled Bare Module Cost ($)
TK-1	**CO_2**	0.844	90	63,500	69,838
TK-2	**H_2 (2)**	39.6	180	127,000	139,677
TK-3	**O_2**	23.7	90	63,500	69,838
TK-4	**LN_2**	0.014	90	63,500	69,838
TK-5	**Glycol/Water**	0.004	90	63,500	69,838
TK-6	**Inerts**	0.011	90	63,500	69,838

Table 5.3.5. Process Cooling Fluid Capital Costs

Cooling Fluid	Volume (m^3)	Cost ($)
LN_2*	70	35,000
Glycol/Water**	29	206,857

** Cost based on a basis of 500 $/m^3 (Fan, 2007)*

*** Cost based on a basis of 7,133 $/m^3 (Yamaha, 2020)*

Table 5.3.6. Capital Costs of Process Consumables

Consumables	Cost ($)
YSZ Catalyst (2 beds) (22,896 kg)*	3,182,544
ICI Catalyst 52-1 (216 kg)**	117,504
Zeolite 3A (24 kg)***	936
Alumina Silica Sodia Sorbent (240 kg)****	23,520

Note: Miscellaneous backup parts are not included and are considered out of scope for the current project.

** Cost based on a basis of 139 $/kg (Inframat, n.d.)*

*** Cost based on a basis of 544 $/kg (Sigma Aldrich, 2020)*

**** Cost based on a basis of 39 $/kg (AlboChemicals, 2020)*

***** Cost based on a basis of 98 $/kg alumina, as the sorbent is 92 wt% alumina (Sigma Aldrich, 2020)*

5.4 Operating Costs

The only significant operating cost in the current process is that of astronaut labor. Based on a time value of $20,000 per astronaut hour, 2 astronauts working continuously on the process, and an operating time of 13,000 hours per cycle for 12 cycles, the total operating cost is $6.24 billion (Reiter, 1996).

Alternatively, the plant could be remotely controlled from Earth. The unit operations could be designed with sensors that would transmit data back to Earth for oversight. This would introduce an eight minute delay, but could be deemed acceptable with the astronauts available in the case of an emergency. It would also require design of such transmission technology, which is outside the scope of this project. In this scenario, the Earth team would manage operational hours (12,000 hr/cycle), while the astronauts would handle maintenance (1,000 hr/cycle). Assuming a pay rate of $100 per hour per operator and 2 operators on Earth, and 2 astronauts performing maintenance, the operational costs across 12 cycles would be $254 million.

A hybrid system could also be proposed, in which the astronauts occasionally take over the operational hours to verify the operation to the Earth team. This would result in an intermediate pricing and help reduce some of the risk of a completely Earth-monitored process.

5.5 Overall Cost Analysis Conclusions

We can compare the cost of producing hydrogen, oxygen, and water using ISRU over the life of the process to shipping costs from Earth over the same time frame. The direct shipping costs can be seen in Table 5.5.1. With a total of $9.8 billion of hydrogen, oxygen, and water, our shipping costs are greatly reduced through the use of ISRU. Including labor costs, covered in section 5.4, the total process could cost anywhere from $7.6 billion to $1.6 billion, resulting in anywhere from $2.2 billion to $8.2 billion in savings through our process. Therefore, the proposed ISRU process is cost effective given the lifetime of the plant.

Table 5.5.1. Costs of Fuel and Water Shipment to Mars

Product	Production Rate (kg/hr)	Total Mass (kg)	Mass after Losses (kg)	Price to Ship from Earth per cycle ($)	Total Price to Ship from Earth ($)	Cost to Purchase on Earth ($)
Hydrogen	0.30	3,600	3,304	66.1 million	0.79 billion	18,200
Oxygen	2.38	28,560	26,212	524.2 million	6.30 billion	6,000
Water	0.94	11,280	11,280	225.6 million	2.71 billion	11

Note: Hydrogen and oxygen are assumed to have 8.22% weight losses due to evaporation, based on predictions of the efficiency of future cooling technology by NASA (NASA, 2008). The production time is 12,000 hours per cycle. Pricing is based on a transportation cost of $20,000/kg mass from Earth. The lifetime of the factory is assumed to be 18 years (144,000 hours).

6. Safety & Environmental Considerations

The biggest safety concern in this process is the contamination of hydrogen or oxygen. These product streams need to remain pure without any cross contamination. If they are accidentally mixed in the wrong place and/or at the wrong time with another substance, it might be a disaster. For instance, hydrogen is very flammable in the presence of oxygen. Furthermore, any carbon monoxide present in the oxygen would poison it for use as fuel or for the biome. Also, any oxygen contamination in the WGS reactor would interfere with the desired reaction, and could even lead to disaster. Other cases of cross contamination that could cause problems include water contamination involving any of the cold materials like liquid nitrogen or glycol/water.

Mechanical safety issues include pressure buildup in the tanks, pipes, and pressure swing adsorbers. The pressure buildup is accounted for with the implementation of emergency outlets. In terms of the compressors, their mechanical parts require appropriate training to maintain and repair. All of the reactors and unit operations are grounded to prevent the buildup of static electricity from gas-solid or liquid-liquid interfaces (Louvar & Crowl, 2019). When reloading the catalyst, the reactors should be clean and dry because any foreign contamination would cause complications during their operation (European Catalyst Manufacturers Association, 2018). The basis of ethical environmental decisions on Mars is a bit different from that on Earth. Since Mars is an inhospitable planet, which may or may not be home to early forms of biological life, it is debatable whether or not it is ethically permissible to pollute a new world. Currently, this process is designed to purge excess CO and CO_2 to the atmosphere and send waste brine to the soil. Since the Martian atmosphere is 95% CO_2, the CO/CO_2 purge to the atmosphere seems to be reasonable; the amount of CO is negligible and the Martian atmosphere is very thin. There might also be H_2 evaporated

during the lifetime of the plant, which has a high probability to leave the atmosphere due to its small mass (compare to how Earth is continually losing H_2). In terms of the salts, the waste stream only consists of salts and water found on Mars, so it could be disposed of in a restricted area.

The astronaut biome is another significant element, but it is outside the scope of the project. It would require its own environmentally-conscious design decisions. The drilling system, required for the retrieval of ice in our process, is intended to be designed by mechanical engineers; there is the issue of how "environmentally safe" it needs to be because drilling and mining are known to have adverse environmental impacts on Earth. This process is designed to be powered by NASA's Kilopower system, which is renewable; it is a nuclear reactor unit with solar panels on top (Hall, 2017).

7. Social Considerations

A manned expedition to Mars would have important implications for society on Earth. The primary societal advantages of a manned Mars mission would be massive gains in scientific data about Mars, technological advances related to the mission, and inspiration for young generations to pursue higher education in Science, Technology, Engineering, and Mathematics (STEM) fields. Furthermore, a human mission to Mars could be the start of the first permanent extraterrestrial colony. However, the main societal disadvantages of such a mission include the uncertainty of the expedition's success and the significant funding required for it that could potentially be used for solving problems on Earth.

Societal Benefits of a Manned Mars Mission

One advantage of a manned Mars mission over a robotic one is the large increase in data collection capability. In this regard, Ehlmann et al. (2005) argue that a human researcher on Mars could operate hundreds of pieces of equipment, compared to rovers that can operate an average of six instruments. Such an increase in data would allow astonishing advances in scientific research regarding not only Mars, but also potentially about the development of microbial life on Earth. A human mission to Mars would also facilitate the development and spread of many of the required technologies to applications on Earth. Fields that would benefit from these technologies include robotics, medicine, and energy use and storage. A summary of these potential technological developments and applications is compiled by Ehlmann et al. (2005) and is seen in Table 6.1.

Table 6.1. Areas of Technology Development from a Manned Mars Mission (Ehlmann et al.)

Challenge to a human Mars mission	Technology development	Terrestrial applications
Harmful effects of microgravity and radiation on human health.	Pharmacological and mechanical prevention treatments.	Prevention, detection, and treatment of illnesses ranging from osteoporosis to cancer.
Limited air, water, and food resources.	Closed loop life-support systems.	Conservation, recycling, waste management.
Limited energy supply.	Alternative energy sources low energy use technologies.	Renewable efficient energy sources; energy conserving consumer products.
Human safety and health is threatened in space.	Automation and robotics.	Remote or automated robotics to reduce human risk in hazardous environments.
Hardware impaired by extreme conditions of space.	Extended life, low maintenance materials, hardware, and systems.	Stronger, smaller, more reliable products for consumers.

A third advantage of a human mission to Mars is inspiration of younger generations to pursue higher education in STEM fields. Joyce et al. (2009) found that the number of students pursuing science and engineering fields was correlated to NASA's budget during the Apollo era in the 1960s. They argue that the funds spent on a human mission to Mars would have similar effects in motivating students to pursue such fields and have economic payoffs in terms of job growth in STEM fields.

Societal Disadvantages of a Manned Mars Mission

One disadvantage of a manned expedition to Mars is the high uncertainty of mission success. Szocik (2018) argues that due to this uncertainty, private investors are unlikely to invest in

a manned Mars mission. He also claims that robotic exploration of Mars is far safer, more effective, and more economically feasible than human exploration. Additionally, settlement of Mars for the survival of humanity in the next several decades, or even centuries, is unreliable, as it would require a long term colony with thousands of residents. A further disadvantage of a manned Mars mission is the large funding requirement. Taylor (2009) estimates a minimum total mission cost of $500 billion. Thrash (2004) claims that the public perceives such costs as financially wasteful, irrelevant, and non-beneficial to Earth-based issues. It will be necessary to inform the public of the importance and benefits of a manned Mars mission to ensure adequate private investment.

8. Conclusions & Recommendations

Conclusions

The current process design resolves issues that arise with shipping all necessary fuel and potable water to Mars. Implementing this process would save $2.2 billion to $8.2 billion, as the materials already present on Mars would be used to satisfy a colony's needs, as opposed to paying to deliver the weight of the same materials from Earth. The concept of Mars ISRU has existed since initial mission plans from as early as 1969, but as of 2020 the current project has approached this process with knowledge of the currently available state of the art technology (von Braun, 1969).

The goal of the current process is to produce enough hydrogen and oxygen for a return trip from Mars, based on the assumption that the ascent vehicle rockets would be propelled by liquid hydrogen fuel since it is most energy efficient, even though alkane fuels have been historically used in past launches. Liquid hydrogen storage can be very costly due to the necessity of cryogenic cooling, which is a reason for the general avoidance of hydrogen fuel. However, the current method of adsorbing the hydrogen to a graphene mesh resolves this issue.

The oxygen would be a product of a CO_2 reducer and the hydrogen would result from the WGS reaction. The water for the reaction would be mined from the Martian regolith, and excess water will be directed to the colony's biome. Thus, this reaction would be able to sustain life on Mars as well as provide a fuel source for an Earth-bound journey.

The social implications of such an undertaking would be seen on a global scale because missions could provide a look into our solar system's past with data collection, as well as possibilities for the future when looking at colonization beyond Earth. However, the environmental concerns do not have as positive of an outlook when the current process is examined. Waste

streams of salts and CO/CO_2 would contaminate the uninhabited planet, which is not a good first impression no matter how small the scale of contamination. This is important considering the first mission would set the precedent for the future. Thus it is important to address areas of concern in the early stages of design, which is why the following section outlines areas that deserve to have more time and effort into application.

Recommendations

We provide several recommendations for improvements and follow up based on our work. The CO_2 reducer took the most amount of time and effort to design, with the level of complexity the highest of the design components. We recommend revisiting this system to perform a more in-depth analysis. This would include optimization of the reaction geometry - in terms of the layers, as our cathode calculations assumed a cylinder - as well as the use of new literature with higher conversions to scale from. Moreover, the water-gas shift reactor reaches its final conversion at about halfway through the reactor, which could be further optimized. A third improvement applies to both reactors. New literature could provide better catalysts and regeneration methods for either reactor, which would greatly reduce their weight requirements. As the unit weights currently drive our economics, getting them as low as possible is a must. Additionally, the reactors were designed to the specific temperature and pressure of the reaction, in order to improve safety it would be recommended to design these reactors as well as our tanks with a higher maximum allowable working pressure (MAWP). This would allow for an inherently safer design in the case of overpressure due to unprecedented varying flow rates, temperature fluxes, or pressure changes.

The dehumidifier water outlet was assumed to be liquid in our project based on the work of Lalik et al. (2006), but further investigation would be necessary to confirm this, as regeneration of

the adsorbent could vaporize the water product. We had difficulties adjusting the cooling and compression duties in order to produce sufficient liquid water for the water recycle system, so we recommend future optimization of heat integration and compression cycles. If the water is actually in the vapor state, a condenser would be required to convert it to liquid water for the human biome. The membrane separator requires further study on methods to achieve complete hydrogen permeation through the membrane, such as increasing the feed pressure, using multiple membranes in series, or adding additional separation elements to drive separation. Another improvement is a lower temperature membrane separator. Our separator runs at 450 ºC for it to be resistant to CO deposition. A better design with higher resistance to CO deposition at temperatures lower than 450 ºC would lower the power necessary for heating. In addition, if some of the compressors were to be combined to optimize the pressure profile of the process, the mass requirement would be minimized. Finally, we recommend optimizing the heat exchanger systems and use of liquid nitrogen. Our heat exchangers were designed in the process of other designs, so they use streams picked arbitrarily. An analysis that uses the heat more effectively to reduce exchanger size and inducer needs would benefit this work. Additionally, removing the antifreeze entirely and optimizing liquid nitrogen use would make the cooling components and weights of the Creare unit lower. As for the tanks, this paper assumed one to two tanks would be needed to store the necessary compounds, while in reality, the dimensions of the tanks would be designated by the engineers who design the rocket that would take the supplies to Mars, and thus the number of tanks needed would be based off of those requirements.

Other recommendations revolve around technological improvements. The first issue is heating and insulation. Most of our heating systems were designed based on current terrestrial

inducer systems. There may be designs for lighter heating systems better suited for space applications. This also applies to the materials of construction, as better casing could be selected to reduce weight. Similarly, our insulation decisions were based solely on aluminized Mylar. A new optimized material, or system of materials, may improve the performance and weight of our designs. Additionally, the insulation was only considered on a few unit operations, so an in-depth analysis over the whole process is required. Finally, our materials of construction were based on materials commonly used on Earth. While some alloys were selected from NASA documents, a greater portion of our materials of construction could receive the same analysis, choosing alloys that perfectly fit the temperature and strain demands while reducing weight.

Our final recommendations involve the scope of the work. This process was focused on separating hydrogen and oxygen to fuel a return trip; however, the topic of the colony's biome was glossed over. A more complete picture of how the habitat interacts with the water and oxygen systems would lead to a better designed facility to meet those demands. Additionally, understanding the size and weight will play a major role in this work's economic viability. Similarly, we did not design the mining system for our salty ice. This would be left to mechanical engineers to design, but understanding the cost and weight is another economic factor. The assembly of the chemical process was also taken for granted, therefore a future study could focus on the robots and/or man labor needed to get the system up and running. To improve the pressure relief system, a pressure vessel may be considered instead of pressure relief valves. The former may provide improved relief, but would incur higher shipment costs due to its greater mass. This safety and cost trade off would need to be considered to determine an optimal pressure relief method. We also recommend designing a more environmentally-friendly system. Considering we are releasing more concentrated

levels of CO back into the atmosphere and leaving the unevaporated salts behind, a better system to deal with these waste streams would be an important design to reduce the human impact on the Martian surface, atmosphere, and potential microbial life.

9. Acknowledgements

We would like to thank our advisor, Professor Eric Anderson of the Chemical Engineering Department, for his continuous support and assistance throughout the project. Our team would also like to thank Professors Geoffrey Geise and Ron Unnerstall of the Chemical Engineering Department for their advice and expertise.

10. References

AlboChemicals. (n.d.). “HFS (R) Molecular Sieve Zeolite 3A 8X12m (1lbs).” *Albochemicals*. (https://www.albochem.com/product/hfs-r-molecular-sieve-zeolite-3a-8x12m-1lbs/).

Alique, D., Martinez-Diaz, D., Sanz, R., & Calles, J. A. (2018). Review of Supported Pd-Based Membranes Preparation by Electroless Plating for Ultra-Pure Hydrogen Production. *Membranes*, *8*(1). https://doi.org/10.3390/membranes8010005

Baburin, Igor A., Alexey Klechikov, Guillaume Mercier, Alexandr Talyzin, and Gotthard Seifert. 2015. “Hydrogen Adsorption by Perforated Graphene.” International Journal of Hydrogen Energy 40(20):6594–99.

Braeunig, R. A. (2012). Rocket Propulsion. http://www.braeunig.us/space/propuls.htm

Briskheat. (2020). *(Full-Coverage Drum Heaters (FGDH/FGPDH/FGDDC)—Drum Heater / Barrel Heater & Insulators—Container Heaters—Heaters—Shop Online* https://www.briskheat.com/products/heaters/drum-container-heaters/drum-pail-heaters-insulators/full-coverage-drum-heaters-fgdh-fgpdh-fgddc-3991.html

Burkhanov, G. (2011). Palladium-Based Alloy Membranes for Separation of High Purity Hydrogen from Hydrogen-Containing Gas Mixtures. Johnson Matthey Technology Review website: https://www.technology.matthey.com/article/55/1/3-12/

Callaghan, C. A. (2006). Kinetics and Catalysis of the Water-Gas-Shift Reaction: A Microkinetic and Graph Theoretic Approach [Worcester Polytechnic Institute]. https://web.wpi.edu/Pubs/ETD/Available/etd-050406-023806/unrestricted/ccallaghan.pdf

Campbell, D. (2019). Personal Communication.

Clark, B. C., & Van Hart, D. C. (1981). The salts of Mars. *Icarus*, *45*(2), 370–378. https://doi.org/10.1016/0019-1035(81)90041-5

Creare (2017). *(DBA Creare)—GovTribe*. https://govtribe.com/vendors/creare-llc-creare-8a287

Davis, M., & Davis, R. (2003). *Fundamentals of Chemical Reaction Engineering*. McGraw-Hill Higher Education.

Dipu, A. L., Ujisawa, Y., Ryu, J., & Kato, Y. (2015). Electrolysis of carbon dioxide for carbon monoxide production in a tubular solid oxide electrolysis cell. *Annals of Nuclear Energy*, *81*, 257–262. https://doi.org/10.1016/j.anucene.2015.02.046

Dunmore. n.d. “Multi Layer Insulation & Multilayer Film Materials | Dunmore.” https://www.dunmore.com/products/multi-layer-films.html

Ebbesen, S. D. and Mogensen, M. (2009). “Electrolysis of Carbon Dioxide in Solid Oxide Electrolysis Cells.” Journal of Power Sources 193(1):349–58.

Economic indicators. (2020). Chemical Engineering 127, (2) (02): 56, http://proxy01.its.virginia.edu/login?url=https://search.proquest.com/docview/2354854738?accountid=14678

Ehlmann, B. L., Chowdhury, J., Marzullo, T. C., Eric Collins, R., Litzenberger, J., Ibsen, S., … Douglas Grant, F. (2005). Humans to Mars: A feasibility and cost–benefit analysis. Acta Astronautica, 56(9), 851–858. https://doi.org/10.1016/j.actaastro.2005.01.010

Eigenberger, G. (2000). Fixed‐Bed Reactors. In Ullmann's Encyclopedia of Industrial Chemistry, (Ed.). doi:10.1002/14356007.b04_199

ElectroHeat. (2020). *Heat treatment and industrial furnaces*. https://www.electroheat.com/

European Catalyst Manufacturers Association. (2018). *Catalyst handling best practice guide*. Cefic. https://www.catalystseurope.eu/images/Documents/ECMA1004q_-_Catalyst_handling_best_practice_guide.pdf

Fan, K. (2007). “Price of Liquid Nitrogen - The Physics Factbook.” (https://hypertextbook.com/facts/2007/KarenFan.shtml).

Gorman-Rupp. n.d. “O Series®.” (https://www.grpumps.com/product/pump/O-Series).

Grace-Davidson. (2010). Adsorbents for Process Applications. https://grace.com/general-industrial/en-us/Documents/sylobead_br_E_2010_f100222_web.pdf

Graco. n.d. “Graco APEX On-Demand Dispensing Pumps.” Retrieved March 9, 2020 (https://www.graco.com/gb/en/products/petroleum-management/apex-on-demand-dispensing-systems.html).

Green, D. W., & Perry, R. H. (2018). Perry's Chemical Engineers' HandbookPerry's Chemical Engineers' Handbook (8 ed.).

Hall, L. (2017). *Kilopower* [Text]. NASA. http://www.nasa.gov/directorates/spacetech/kilopower

Hall, L. (2017). “Planting an Ecosystem on Mars.” NASA. http://www.nasa.gov/feature/planting-an-ecosystem-on-mars.

Haynes International. (2015). “Nominal Composition.” (http://www.haynesintl.com/alloys/alloy-portfolio_/Corrosion-resistant-Alloys/HASTELLOY-C-276-Alloy/nominal-composition).

Hu, X., & Xie, K. (2019). Active and stable Ni/Cr2O3-δ cathodes for high temperature CO2 electrolysis. *Journal of Power Sources*, *430*, 20–24. https://doi.org/10.1016/j.jpowsour.2019.05.014

Hussaro, K.; Douglas, S.; Cheamsawat, N. Synthesis of Zeolite from Aluminium Etching By-Product: The Effect of Reaction Temperature on Crystallinity and Its CO2 Adsorption Property. Am. J. Environ. Sci. 2008, 4 (6), 666–674. https://doi.org/10.3844/ajessp.2008.666.674.

Inframat. (n.d.). "8mol% Yttria Stabilized Zirconia (YSZ) Powder Superfine Grade." (http://www.inframat.com/products/4039OR-8601.htm).

Japan Pionics Co., Ltd. (2010). Palladium Alloy Membrane Permeation Hydrogen Gas Purifier. http://www.japan-pionics.co.jp/en/product/refine/refine_hydrogen.html

Joyce, S., Ferguson, C., & Weinstein, P. (2009). Public support for Mars missions: The importance of informing the next generation. Acta Astronautica, 64(7), 718–723. https://doi.org/10.1016/j.actaastro.2008.12.014

King, P. L., & Mclennan, S. M. (2010). Sulfur on Mars. *Elements*, *6*(2), 107–112. doi: 10.2113/gselements.6.2.107

Kleinhenz, J. (2017). *An ISRU Propellant Production System to Fully Fuel a Mars Ascent Vehicle*. https://ntrs.nasa.gov/search.jsp?R=20170005179

L&W Compressors. n.d. "LW 230 E Compact | L&W Compressors." Retrieved March 8, 2020 (https://www.lw-compressors.com/node/27).

Lalik, E., Mirek, R., Rakoczy, J., & Groszek, A. (2006). Microcalorimetric study of sorption of water and ethanol in zeolites 3A and 5A. Catalysis Today, 114(2), 242–247. https://doi.org/10.1016/j.cattod.2006.01.006

LaRC, B. A. (n.d.). NASA - Human Needs: Sustaining Life During Exploration. https://www.nasa.gov/vision/earth/everydaylife/jamestown-needs-fs.html

Lee, J. A. (2016). *United States Patent: 9284636 - Impact toughness and heat treatment for cast aluminum* (Patent No. 9284636). http://patft.uspto.gov/netacgi/nph-Parser?Sect1=PTO1&Sect2=HITOFF&d=PALL&p=1&u=%2Fnetahtml%2FPTO%2Fsrchnum.htm&r=1&f=G&l=50&s1=9,284,636.PN.&OS=PN/9,284,636&RS=PN/9,284,636

Legal Information Institute. (n.d.). 49 CFR § 195.106—Internal design pressure. Legal Information Institute website: https://www.law.cornell.edu/cfr/text/49/195.106

Loganathan, A., Shantha, M. S., J, B. S. R., Loganathan, A., & Shantha, M. S. (2010). A Review of the Water Gas Shift Reaction Kinetics. International Journal of Chemical Reactor

Engineering - INT J CHEM REACT ENG, 8. http://citeseerx.ist.psu.edu/viewdoc/download?doi=10.1.1.463.6890&rep=rep1&type=pdf

Louvar, J. F., & Crowl, D. A. (2019). *Chemical Process Safety: Fundamentals with Applications* (4th ed.). Prentice Hall. https://www.oreilly.com/library/view/chemical-process-safety/9780134857893/

Mahoney, E. (2017). *In-Situ Resource Utilization* [Text]. NASA. http://www.nasa.gov/isru

McClure, Patrick Ray (2019). "A small fission reactor for planetary surface and deep space power" (PDF).

Mejdell, A. L., Jøndahl, M., Peters, T. A., Bredesen, R., & Venvik, H. J. (2009). Effects of CO and CO2 on hydrogen permeation through a ~3μm Pd/Ag 23wt.% membrane employed in a microchannel membrane configuration. *Separation and Purification Technology*, *68*(2), 178–184. https://doi.org/10.1016/j.seppur.2009.04.025

Meyen, F. E., Hecht, M. H., & Hoffman, J. A. (2016). Thermodynamic model of Mars Oxygen ISRU Experiment (MOXIE). *Acta Astronautica*, *129*, 82–87. https://doi.org/10.1016/j.actaastro.2016.06.005

Michell Humidity Calculator. n.d. “Michell Humidity Calculator.” http://www.michell.com/us/calculator/.

Munevar, G. (2019). An obligation to colonize outer space. *Futures*, *110*, 38–40. https://doi.org/10.1016/j.futures.2019.02.009

NASA. (2008). Advanced Space Transportation Program: Paving the Highway to Space. https://www.nasa.gov/centers/marshall/news/background/facts/astp.html

NASA.(2008). Cryogenic Fluid Management. https://www.nasa.gov/centers/ames/research/technology-onepagers/cryogenic-fluid-management.html

NASA. (2016). “NASA-427: A New Aluminum Alloy.” https://technology.nasa.gov/patent/MFS-TOPS-8.

NASA. (2018). *Kilopower Press Conference*. https://www.nasa.gov/sites/default/files/atoms/files/kilopower_media_event_charts_16x9_final.pdf

NASA. (2019). *Finding A Place to Land on Mars*. NASA Mars. https://mars.nasa.gov/mro/multimedia/slideshows/findingaplacetolandonmars/

Nikolewski, R. 2018. “NASA Looks to Send a Small Nuclear Reactor to the Moon and Mars.” San

Diego Union-Tribune. https://www.sandiegouniontribune.com/business/energy-green/sd-fi-nasa-nuclear-20180523-story.html.

Orwig, J. (2015). *5 undeniable reasons humans need to colonize Mars—Even though it's going to cost billions*. Business Insider. https://www.businessinsider.com/5-undeniable-reasons-why-humans-should-go-to-mars-2015-4

Paglieri, S. N., & Way, J. D. (2002). Innovations in Palladium Membrane Research. *Separation and Purification Methods*, *31*(1), 1–169. https://doi.org/10.1081/SPM-120006115

Park, Doo-Hwan, Sung-Woong Choi, Jeong-Hyeon Kim, and Jae-Myung Lee. 2015. "Cryogenic Mechanical Behavior of 5000- and 6000-Series Aluminum Alloys: Issues on Application to Offshore Plants." Cryogenics 68:44–58.

Peters, Max Stone, Klaus D. Timmerhaus, and Ronald E. West. 2003. Plant Design and Economics for Chemical Engineers. 5th ed. New York: McGraw-Hill.

Plachta, D. (2017). *Liquid Nitrogen Zero Boiloff Testing*. https://ntrs.nasa.gov/search.jsp?R=20170001537

Powell, J., Maise, G., & Paniagua, J. (2001). Self-sustaining Mars colonies utilizing the North Polar Cap and the Martian atmosphere. *Acta Astronautica*, *48*(5–12), 737–765. https://doi.org/10.1016/s0094-5765(01)00081-9

Quincy Compressor. (2012). QGS. *Quincy Compressor*. https://www.quincycompressor.com/products/rotary-screw-air-compressors/qgs/

Ralphs, M., Franz, B., Baker, T., & Howe, S. (2015). Water extraction on Mars for an expanding human colony. *Life Sciences in Space Research*, *7*, 57–60. https://doi.org/10.1016/j.lssr.2015.10.001

Reiter, R. J. (1996). Melatonin. Bantam Books.

Ross, R. G. Quantifying MLI Thermal Conduction in Cryogenic Applications from Experimental Data. IOP Conf. Ser. Mater. Sci. Eng. 2015, 101, 012017. https://doi.org/10.1088/1757-899X/101/1/012017.

Salmi, T., & Hakkarainen, R. (1989). Kinetic Study of the Low-Temperature Water-Gas Shift Reaction over a Cu—ZnO Catalyst. Applied Catalysis, 49(2), 285–306. https://doi.org/10.1016/S0166-9834(00)83024-9

Sánchez, J. M., Barreiro, M. M., & Maroño, M. (2014). Bench-scale study of separation of hydrogen from gasification gases using a palladium-based membrane reactor. *Fuel*, *116*, 894–903. https://doi.org/10.1016/j.fuel.2013.02.051

Sciencing. (2018). Price of Galvanized Steel Vs. Stainless Steel. https://sciencing.com/about-6711987-price-steel-vs--stainless-steel.html

Shao, W.; Zhang, L.; Li, L.; Lee, R. L. Adsorption of CO2 and N2 on Synthesized NaY Zeolite at High Temperatures. Adsorption 2009, 15 (5), 497. https://doi.org/10.1007/s10450-009-9200-y.

Sharp, T. (2017). What is the Temperature of Mars? Space.Com. https://www.space.com/16907-what-is-the-temperature-of-mars.html

Shishko, R., Fradet, R., Saydam, S., Dempster, A., & Coulton, J. (2015). An Integrated Economics Model for ISRU in Support of a Mars Colony–Initial Status Report. In *AIAA SPACE 2015 Conference and Exposition*. American Institute of Aeronautics and Astronautics. https://doi.org/10.2514/6.2015-4564

Sigma Aldrich. (2020). "Aluminum Oxide 199974." Al2O3. (https://www.sigmaaldrich.com/catalog/product/sigald/199974).

Sigma Aldrich. (2020). *Copper (Cu) Catalysts*. https://www.sigmaaldrich.com/chemistry/chemistry-products.html?TablePage=16245043

Sigma Aldrich. (2020). Palladium 203939. (2020). https://www.sigmaaldrich.com/catalog/product/aldrich/203939

Sigma Aldrich. (2020). Yttrium 261327. (2020). https://www.sigmaaldrich.com/catalog/product/aldrich/261327

Smith, B., Muruganandam, L., Murthy, L., & Shantha, S. (2010). A Review of the Water Gas Shift Reaction Kinetics. International Journal of Chemical Reactor Engineering - INT J CHEM REACT ENG, 8. https://doi.org/10.2202/1542-6580.2238

Smith, K., & Abney, K. (2019). Human colonization: A world too far? *Futures*, *110*, 1–3. https://doi.org/10.1016/j.futures.2019.02.003

Smith, K. C., Abney, K., Anderson, G., Billings, L., Devito, C. L., Patrick Green, B., Johnson, A. R., Marino, L., Munevar, G., Oman-Reagan, M. P., Potthast, A., Schwartz, J. S. J., Tachibana, K., Traphagan, J. W., & Wells-Jensen, S. (2019). The Great Colonization Debate. *Futures*, *110*, 4–14. https://doi.org/10.1016/j.futures.2019.02.004

SpaceX. (2016). *Mars* [Text]. SpaceX. https://www.spacex.com/mars

Szocik, K. (2018). Should and could humans go to Mars? Yes, but not now and not in the near future. Futures, 105, 54-66.

Taylor, F. W. (2009). The Scientific Exploration of Mars: Cambridge University Press.

Thrash, T. A. (2004). Space Education and Public Relations: What Goes Up Must Stay Down. Paper presented at the Space 2004 Conference and Exhibit, San Diego, California. https://arc.aiaa.org/doi/abs/10.2514/6.2004-6075

Turton, R. (Ed.). (2009). Analysis, synthesis, and design of chemical processes (3rd ed). Upper Saddle River, N.J: Prentice Hall.

Twigg, M. V. (2018). Catalyst Handbook. Routledge.

Von Braun, W. (1965). Popular Science. Bonnier Corporation.

von Braun, W. (1969). Manned Mars Landing - Presentation to the Space Task Group. https://www.nasa.gov/sites/default/files/atoms/files/19690804_manned_mars_landing_presentation_to_the_space_task_group_by_dr._wernher_von_braun.pdf: National Aeronautics and Space Administration

Walton, K. S., & LeVan, M. D. (2006). A Novel Adsorption Cycle for CO Recovery: Experimental and Theoretical Investigations of a Temperature Swing Compression Process. *Separation Science and Technology*, *41*(3), 485–500. https://doi.org/10.1080/01496390500524834

Wankat, P. C. (2012). *Separation process engineering: Includes mass transfer analysis* (3rd ed). Prentice Hall.

Wasilewski, T. G. (2018). Evaluation of drilling-based water extraction methods for Martian ISRU from mid-latitude ice resources. *Planetary and Space Science*, *158*, 16–24. https://doi.org/10.1016/j.pss.2018.05.012

Wiedemann, D. (2014). *Water Recycling* [Text]. NASA. http://www.nasa.gov/content/water-recycling

Yamaha. (2020). Yamacool High-Performance Antifreeze. https://www.shopyamaha.com/product/details/yamacool-high-performance-antifreeze

Yin, Z., Palmore, G. T. R., & Sun, S. (2019). Electrochemical Reduction of CO2 Catalyzed by Metal Nanocatalysts. *Trends in Chemistry*, *0*(0). https://doi.org/10.1016/j.trechm.2019.05.004

Yurkiv, V., Starukhin, D., Volpp, H.-R., & Bessler, W. G. (2011). Elementary Reaction Kinetics of the CO/CO2/Ni/YSZ Electrode. *Journal of The Electrochemical Society*, *158*(1), B5–B10. https://doi.org/10.1149/1.3505296

Appendix A: Nomenclature

u	Stream velocity
C_i	Concentration of component i
z	Length along reactor
η_o	Overall effectiveness factor
ρ_b	Catalyst bed density
ν_i	Stoichiometric coefficient of component i
r	Reaction rate
ρ	Stream density
C_p	Heat capacity
T	System temperature
ΔH_r	Enthalpy of reaction
T^0	Initial stream temperature
U	Overall heat transfer coefficient
d_t	Reactor tube diameter
T^*	Reference temperature
P	System pressure
f_f	Friction factor
g_c	Gravitational acceleration
d_p	Particle diameter
C_i^0	Initial inlet concentration
P^0	Initial system pressure
H_i	Enthalpy of component i
S_i	Entropy of component i

$k_{f,2}$	Reaction rate constant
K_3	Reaction equilibrium constant
K_1	Reaction equilibrium constant
K_4	Reaction equilibrium constant
K_{01}	Reaction equilibrium constant
Re	Reynolds number
ν	Kinematic viscosity
d	Tube diameter
Nu	Nusselt number
Pr	Prandtl number
h	Convective heat transfer coefficient
k	Thermal conductivity of fluid
p	Partial pressure
α	Reaction rate order
β	Reaction rate order
K_{eq}	Reaction equilibrium constant
n_{per}	Permeate flux
P	Permeability
P_{ret}	Retentate pressure
P_{per}	Permeate pressure
t	Membrane thickness
ΔT_c	Cold stream temperature difference
ΔT_h	Hot stream temperature difference
t	Tank wall thickness
P	Tank internal pressure

d	Inner tank wall diameter
S	Yield strength
E	Seam joint factor
F	Design factor
q	Heat transfer rate
S.A.	Surface area
r_i	Inner tank radius
L	Tank height
V	Vessel volume
A	Heat transfer area
P	Vessel pressure

Appendix B: Sample Calculations

See the zipped folder for the *Supplemental Files*.